Coordination-Driven Self-Assembly, Structures, and Dynamic Properties of Diplatinum Hexatriynediyl and Butadiynediyl Complexes in which the sp Carbon Chains are Shielded by sp³ Carbon Chains: Towards Endgroup–Endgroup Interactions

Gareth R. Owen,[a] Jürgen Stahl,[a] Frank Hampel,[a] and John A. Gladysz*[a, b]

Abstract: Sequential reactions of *trans*-$(C_6F_5)(p\text{-tol}_3P)_2Pt(C\equiv C)_3SiEt_3$ (**PtC₆-SiEt₃**) with $n\text{Bu}_4N^+ F^-$ (THF/methanol), **PtCl**, $KPF_6/t\text{BuOK}$, and CuCl give *trans,trans*-$[(C_6F_5)\{(p\text{-tol}_3P)_2\}Pt(C\equiv C)_3Pt\{(Pp\text{-tol}_3)_2\}(C_6F_5)]$ (**PtC₆Pt**) in 95% yield on multigram scales. Reactions of **PtC₆Pt** and $Ar_2P(CH_2)_mPAr_2$ afford substitution products *trans,trans*-$[(C_6F_5)\{(Ar_2P(CH_2)_mPAr_2)\}Pt(C\equiv C)_3Pt\{(Ar_2P(CH_2)_m PAr_2)\}(C_6F_5)]$ (**PtC₆Pt-*m*/Ar**; *m*/Ar = 8/*p*-tol, 78%; 10/Ph, 82%; 11/Ph, 69%; 12/Ph, 57%; 14/*p*-tol, 57%; 14/*p*-C_6H_4-*t*Bu, 71%), in which the diphosphines span the square planar platinum endgroups. An analogous reaction with PEt₃ gives a tetrakis PEt₃ complex **Pt′C₆Pt′** (72%). The crystal structures of **PtC₆Pt**, **Pt′C₆Pt′**, **PtC₆Pt-10/Ph**, **PtC₆Pt-11/Ph**, and **PtC₆Pt-14/*p*-tol** or solvates thereof are compared. In **PtC₆Pt**, the endgroups can avoid van der Waals contact, and define angles of 0°. In **PtC₆Pt-14/*p*-tol**, the sp³ chains twist around the sp chain in a chiral double-helical motif, with an endgroup/endgroup angle of 189°. The sp³ chains are too short to adopt analogous conformations in the other complexes, but laterally shield the sp chain. NMR spectroscopy shows that the helical enantiomers of **PtC₆Pt-14/*p*-tol** rapidly interconvert in solution at low temperature. A crystal structure of **PtC₄Pt** shows endgroups that are in van der Waals contact and define an angle of 41°. Reactions with $Ar_2P(CH_2)_8PAr_2$ give **PtC₄Pt-8/Ar** (Ar = Ph, 53%; *p*-tol, 87%). Low-temperature NMR spectroscopy establish non-helical chiral conformations. Electrochemical oxidations of the diplatinum complexes are analyzed, the reversibilities of which decrease with increasing sp chain length.

Keywords: helical structures · NMR spectroscopy · platinum · self-assembly · structure elucidation

Introduction

Assemblies in which sp carbon chains span two transition metals, $[(L)_yMC_xM'(L')_y]$, have received much attention from both fundamental and applied viewpoints.[1–3] The one-dimensional C_x linkages very efficiently delocalize the odd electrons of radical ions between the metal endgroups.[2] They are much more effective than most other types of unsaturated bridging ligands, which usually can be twisted out of conjugation.[2] The C_x linkages also appear to be extendable to greater lengths[4–6] than in analogs with carbon- or silicon-based endgroups.[7] A $PtC_{28}Pt$ adduct currently holds the "record" for isolable compounds.[6]

As this field grows and evolves, attention is increasingly being directed at "second generation" families of complexes with special architectural features. One example would be polygons; squares with Pt_4C_{16} cores have been reported by Youngs, Bruce, and Anderson.[8] Among our own efforts, we have described extensive series of diplatinum polyynediyl or $[Pt(C\equiv C)_nPt]$ complexes ($n = 2, 3, 4, 5, 6, 8, 10, 12, 14$).[5, 6, 9, 10] These have been covalently linked in lateral arrays ("bundles")[11] and longitudinal arrays (e.g., $[Pt(C\equiv C)_4]_nPt$ oligomers).[12]

As summarized in Scheme 1, we have also developed two complementary routes to complexes of the formula *trans,trans*-$[(C_6F_5)\{(Ar_2P(CH_2)_mPAr_2)\}Pt(C\equiv C)_n\{Pt\{(Ar_2P-$

[a] Dr. G. R. Owen, Dr. J. Stahl, Dr. F. Hampel, Prof. Dr. J. A. Gladysz
Institut für Organische Chemie and
Interdisciplinary Center for Molecular Materials
Friedrich-Alexander-Universität Erlangen-Nürnberg
Henkestrasse 42, 91054 Erlangen (Germany)
Fax (+49) 9131-852-6865
E-mail: gladysz@chemie.uni-erlangen.de

[b] Prof. Dr. J. A. Gladysz
Department of Chemistry, Texas A&M University
PO Box 30012, College Station, Texas 77842–3012 (USA)
Fax (+1) 979-845-5629
E-mail: gladysz@mail.chem.tamu.edu
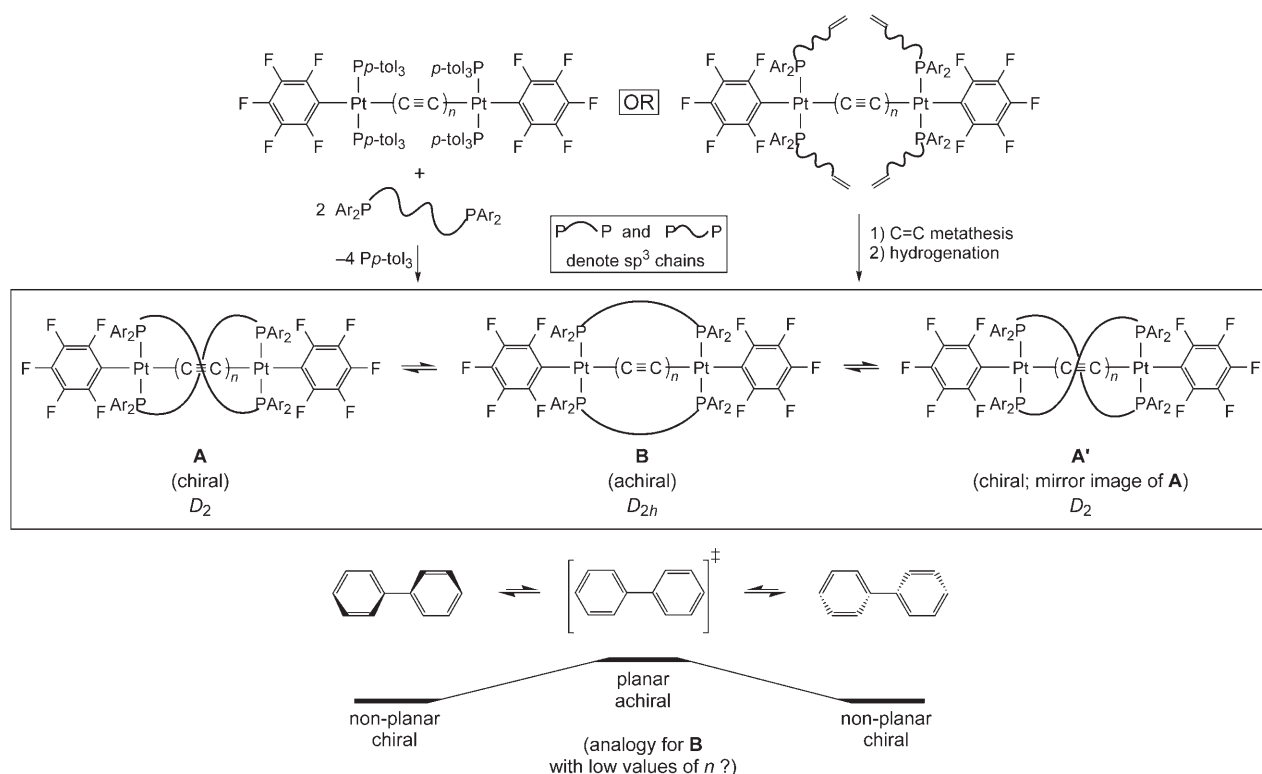
Scheme 1. Syntheses and limiting structures of complexes **PtC$_x$Pt-m/Ar** ($x=2n$) derived from $C_6F_5Pt(C\equiv C)_nPtC_6F_5$ units and termini-spanning α,ω-diphosphines $Ar_2P(CH_2)_mPAr_2$ (top, middle), and approaches to destabilizing conformations with coplanar endgroups such as **B** (bottom).

$(CH_2)_mPAr_2)\}(C_6F_5)]$ (**PtC$_x$Pt-m/Ar**; $x=2n=8$, 12).[13–15] One involves phosphine ligand substitution, or "coordination-driven self-assembly", and the other an alkene metathesis/hydrogenation sequence. The products contain endgroup-spanning α,ω-diphosphines that sterically shield the sp carbon chains. In the cases with m/x/Ar = 14/8/Ph, 14/8/p-tol, 14/8/p-C$_6$H$_4$-tBu, 20/8/Ph, and 18/12/Ph, crystal structures show that the sp^3 carbon chains wrap around the sp chains in striking chiral double-helical conformations **A** that have idealized D_2 symmetry. The corresponding radical cations became longer lived, inviting analogies to "insulated molecular wires".[16] At lower sp^3/sp carbon ratios, formally achiral conformations of the type **B** are observed.

However, it has proved difficult to definitively establish that the conformations **A** dominate in solution. These feature, like most other helical species, a number of diastereotopic groups (e.g., PAr_2, PCH_2). Thus, two sets of NMR signals are observed with many helical molecules.[17] In favorable situations, the two sets coalesce to one at a higher temperature.[17a] This normally requires the "untwisting" of the helix to a formally achiral conformation, and subsequent retwisting to the opposite enantiomer (e.g., **A**→**B**→**A'** in Scheme 1). A net exchange of the diastereotopic groups results.[18]

All complexes of the type **PtC$_x$Pt-m/Ar** investigated to date have exhibited only a single set of NMR signals, even at very low temperatures. Phosphorus–platinum coupling is always observed ($J_{PPt} \approx 2600$ Hz), and this indicates that dis-

sociation of the phosphorus donor atoms is slow. These results are consistent with several possibilities, including a) the rapid interconversion of the enantiomeric double-helical structures **A**/**A'** by untwisting/retwisting mechanisms, or b) a preference for achiral ground states (**B**) in solution. Accordingly, we set out to develop analogs that might exhibit higher barriers to enantiomer interconversion.

In one approach, described elsewhere,[15] the sp^3 chains were functionalized. In a parallel approach, and the subject of this investigation, we sought to extend the above chemistry from PtC$_8$Pt and PtC$_{12}$Pt systems to lower homologues with shorter C$_x$ bridges. It was thought that endgroup–endgroup steric interactions would eventually destabilize the achiral conformation **B** and slow the **A**/**A'** equilibrium. This has abundant precedent with biaryls, which (as illustrated in Scheme 1, bottom) exhibit chiral non-planar ground states that interconvert via achiral planar transition states.[19,20] The barriers can be fine-tuned by introducing *ortho* substituents of varying sizes. Some diarylethynes ArC≡CAr have also been engineered to adopt non-planar conformations.[21,22]

In this paper, we report 1) reactions of the hexatriynediyl complex *trans,trans*-[(C$_6$F$_5$){(p-tol$_3$)P)$_2$}Pt(C≡C)$_3$Pt{(Pp-tol$_3$)$_2$}(C$_6$F$_5$)] (**PtC$_6$Pt**)[5] with longer-chain diphosphines leading to assemblies of the type **A**, 2) reactions of **PtC$_6$Pt** with shorter-chain diphosphines leading to assemblies of the type **B**, 3) parallel chemistry with the butadiynediyl complex **PtC$_4$Pt** leading to assemblies that have chiral ground states in solution but are conformationally distinct from **A**, 4) attendant

crystallographic, variable temperature NMR, and cyclic voltammetry data, and 5) detailed analyses thereof. A portion of this work has been communicated,[23] and additional details can be found elsewhere.[24]

Results

Syntheses and structures of unbridged butadiynediyl and hexatriynediyl complexes: The complexes **PtC$_6$Pt** and **PtC$_4$Pt** have been previously synthesized by means of CuCl-catalyzed cross-couplings of polyynyl complexes **PtC$_x$H** and the chloride complex **PtCl**.[5] During the course of this study, an improved protocol for **PtC$_6$Pt** was developed. As shown in Scheme 2, **PtC$_6$SiEt$_3$** was first combined with the fluoride salt nBu$_4$N$^+$ F$^-$ in protic media to generate the labile complex **PtC$_6$H**. Interestingly, when the CuCl-catalyzed reaction with **PtCl** was conducted in the presence of stoichiometric amounts of KPF$_6$ and tBuOK, the yield of **PtC$_6$Pt** increased from 34% to 95%.[25] Quantities exceeding two grams were easily prepared. No **PtC$_6$Pt** was obtained in the absence of CuCl.

The relative sizes of different endgroups are most easily visualized in adducts with modest endgroup separations. Thus, a sample of **PtC$_6$Pt** was treated with 4.5 equiv of PEt$_3$. As shown in Scheme 2, workup gave the four-fold phosphine substitution product **Pt′C$_6$Pt′** in 72% yield. Analogous reactions of the higher homologues **PtC$_8$Pt** and **PtC$_{12}$Pt** have been reported previously.[5] The new complex **Pt′C$_6$Pt′** and others were normally characterized by NMR (^{1}H, ^{13}C, ^{31}P) and IR spectroscopy, mass spectrometry, and microanalysis, as summarized in the Experimental Section. Unless otherwise noted, spectroscopic properties were similar to those of related complexes described earlier.

Many Pt(C≡C)$_n$Pt species can be crystallized.[3] Accordingly, the crystal structures of **PtC$_4$Pt**, a solvate of **PtC$_6$Pt**, and **Pt′C$_6$Pt′** were determined as summarized in Table 1 and the Experimental Section. Views of the molecular structures, the last two of which exhibit inversion centers at the mid-

points of the sp chains, are presented in Figures 1–3. Key metrical parameters are summarized in Table 2.

In accord with the expectations given in the introduction, the endgroups in **PtC$_4$Pt** were not coplanar, as highlighted in the partial structures in Figure 2. For quantifying endgroup/endgroup angles, we prefer to use the planes defined by the P-Pt-P linkage on one endgroup and the platinum atom on the other. These emphasize the twist defined by the two P-Pt-P linkages, and are less affected by various geometric non-idealities. However, an alternative measure based on the platinum coordination planes is also included in Table 2. The values are usually quite close (41.0°–40.8°) for **PtC$_4$Pt**, but can differ by as much 35° in certain bow-shaped complexes.[13]

In contrast to **PtC$_4$Pt**, the endgroups in **PtC$_6$Pt** were coplanar, as mandated by the inversion center. Both **PtC$_6$Pt** and **PtC$_4$Pt** exhibited the C$_6$H$_4$R/C$_6$F$_5$/C$_6$H$_4$R π-stacking interaction commonly seen in this series of compounds.[5,11,13–15,26] The average centroid–centroid distances are also given in Table 2. Consistent with the inversion center, the endgroups in **Pt′C$_6$Pt′** were also coplanar.[27] The higher homologue **Pt′C$_{12}$Pt′** exhibits an analogous conformation.[5]

As illustrated by the space-filling representations **C** and **D** in Figure 3, there are extensive van der Waals contacts between the endgroups in **PtC$_4$Pt**, which appear to embrace. In contrast, there are no van der Waals contacts in **PtC$_6$Pt** (see **E**, **F**). The shortest hydrogen-hydrogen distance is 2.71 Å. As illustrated by **G** and **H**, the PEt$_3$-substituted endgroups in **Pt′C$_6$Pt′** are distinctly smaller than the Pp-tol$_3$-substituted endgroups in **PtC$_6$Pt**. Significantly more of the sp chain is exposed. For comparison, analogous views of the longer-chain octatetraynediyl complex **PtC$_8$Pt** are provided (**I**, **J**).[5]

Syntheses of bridged hexatriynediyl complexes: Despite the "near miss" with regard to endgroup/endgroup interactions in crystalline **PtC$_6$Pt**, reactions with α,ω-diphosphines were nevertheless investigated. It was hoped that 1) coordination-
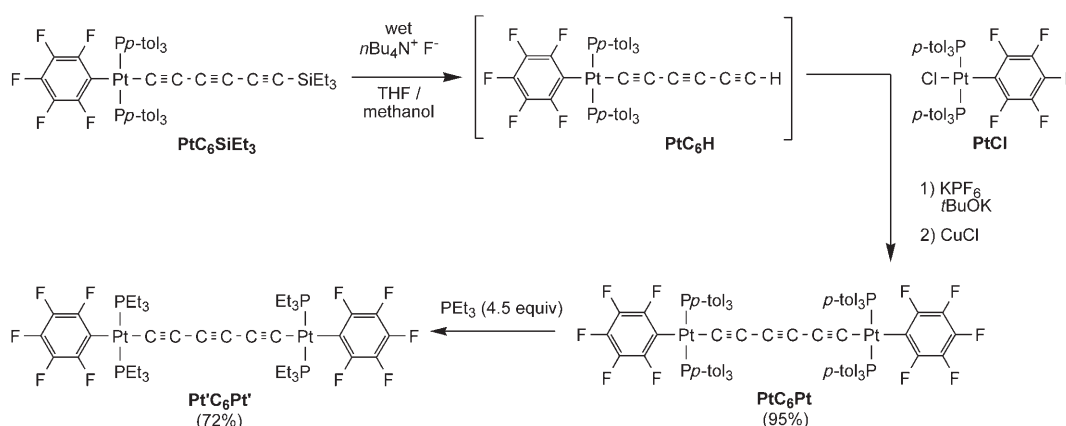
Scheme 2. Syntheses of diplatinum hexatriynediyl complexes **PtC$_6$Pt** and **Pt′C$_6$Pt′**.

Table 1. Summary of crystallographic data.[a]

	PtC$_6$Pt·4THF	Pt'C$_6$Pt'	PtC$_6$Pt-10/Ph	PtC$_6$Pt-11/Ph·2CH$_2$Cl$_2$	PtC$_6$Pt-14/p-tol·2CH$_2$Cl$_2$	PtC$_4$Pt
empirical formula	C$_{118}$H$_{116}$F$_{10}$O$_4$P$_4$Pt$_2$	C$_{42}$H$_{60}$F$_{10}$P$_4$Pt$_2$	C$_{86}$H$_{80}$F$_{10}$P$_4$Pt$_2$	C$_{90}$H$_{88}$Cl$_4$F$_{10}$P$_4$Pt$_2$	C$_{104}$H$_{116}$Cl$_4$F$_{10}$P$_4$Pt$_2$	C$_{100}$H$_{84}$F$_{10}$P$_4$Pt$_2$
formula weight	2302.17	1268.96	1817.56	2015.46	2211.83	1989.73
crystal system	triclinic	monoclinic	monoclinic	triclinic	triclinic	triclinic
space group	P$\bar{1}$	P2$_1$/c	C2/c	P$\bar{1}$	P$\bar{1}$	P2$_1$/n
unit cell dimensions:						
a [Å]	13.4269(2)	15.6304(3)	42.6816(7)	12.5504(2)	15.0284(2)	14.8560(1)
b [Å]	14.8625(3)	11.4513(3)	9.1247(2)	12.5639(2)	18.1876(2)	24.4690(2)
c [Å]	14.9832(2)	13.6613(2)	22.0727(3)	15.6464(2)	21.3651(2)	25.6070(2)
α [°]	104.4233(8)	90	90	73.2385(8)	102.614(6)	90
β [°]	98.3223(9)	91.3330(14)	118.081(11)	73.6865(9)	103.327(6)	108.4530(4)
γ [°]	114.8313(8)	90	90	65.1352(9)	112.551(5)	90
V [Å^3]	2520.08(7)	2444.55(9)	7584.4(2)	2106.86(5)	4932.71(10)	8829.83(12)
Z	1	2	4	1	2	4
ρ calcd [M gm^{-3}]	1.517	1.724	1.592	1.589	1.489	1.497
μ [mm^{-1}]	2.909	5.913	3.839	3.586	3.071	3.305
F(000)	1162	1236	3608	1002	2228	3960
crystal size [mm]	0.20×0.20×0.10	0.15×0.15×0.01	0.30×0.15×0.10	0.20×0.20×0.10	0.30×0.30×0.20	0.30×0.20×0.20
Θ range	1.46 to 27.51	2.20 to 27.47	2.30 to 27.46	1.38 to 27.50	1.51 to 27.50	4.10 to 27.48
index ranges (h,k,l)	−17,17; −19,19; −19,19	−20,20; −14,14; −17,17	−55,55; −11,11; −28,28	−16,16; −16,16; −20,20	−19,19; −23,23; −27,27	−19,19; −31,30; −33,33
reflections collected	21640	10722	16236	18265	42998	34705
independent reflections	11527	5585	8619	9643	22634	20060
R(int)	0.0201	0.0288	0.0259	0.0180	0.0250	0.0428
reflections [I>2σ(I)]	10337	4432	7160	8906	17613	14087
completeness to Θ	99.4% (27.5)	99.9% (27.5)	99.2% (27.5)	99.5% (27.5)	99.8% (27.5)	99.1% (27.5)
data/restraints/parameters	11527/0/622	5585/0/262	8619/0/460	9643/0/496	22634/4/1125	20060/0/1045
goodness-of-fit on F^2	1.066	1.034	1.030	1.115	1.034	1.005
R indices (final) [I>2σ(I)]						
R$_1$	0.0286	0.0306	0.0333	0.0246	0.0303	0.0402
wR$_2$	0.0706	0.0727	0.0820	0.0633	0.0732	0.0923
R indices (all data)						
R$_1$	0.0346	0.0457	0.0450	0.0283	0.0475	0.0701
wR$_2$	0.0772	0.0788	0.0887	0.0691	0.0811	0.1028
largest diff. peak/hole [e Å^{-3}]	1.344/−1.181	1.470/−1.841	1.578/−2.394	0.968/−1.332	1.630/−1.081	4.180/−1.606

[a] Data common to all structures: $T = 173(2)$ K; $\lambda = 0.71073$ Å; refinement method: full-matrix least-squares on F^2; Bruker-AXS Smart 1000 diffractometer.

Table 2. Key crystallographic distances [Å] and angles [°].

	PtC$_6$Pt·4THF[a]	Pt'C$_6$Pt'[a]	PtC$_6$Pt-10/Ph[a]	PtC$_6$Pt-11/Ph·2CH$_2$Cl$_2$[a]	PtC$_6$Pt-14/p-tol·2CH$_2$Cl$_2$	PtC$_4$Pt
Pt⋯Pt	10.3610(3)	10.3829(3)	10.3705(16)	10.2928(2)	10.3966(4)	7.7668(2)
sum of bond lengths, Pt1 to Pt2	10.365	10.388	10.391	10.326	10.404	7.784
Pt1−C1/Pt2−C6	1.995(3)	2.000(4)	1.998(4)	1.986(3)	2.001(3)/2.006(3)	1.986(5)/1.937(7)[b]
C1−C2/C5−C6	1.213(4)	1.213(6)	1.219(6)	1.212(4)	1.226(5)/1.216(5)	1.212(7)/1.272(7)[c]
C2−C3/C4−C5	1.371(4)	1.371(6)	1.376(6)	1.362(4)	1.370(5)/1.364(5)	1.377(7)[d]
C3−C4	1.207(6)	1.220(9)	1.205(8)	1.206(6)	1.221(5)	–
Pt1-C1-C2/Pt2-C6-C5	177.4(3)	178.5(4)	174.5(4)	173.6(3)	175.8(3)/178.5(3)	174.7(4)/172.7(4)[e]
C1-C2-C3/C6-C5-C4	178.7(4)	178.6(5)	177.2(5)	176.0(3)	178.8(4)/177.6(4)	176.1(5)/178.8(6)[f]
C2-C3-C4/C5-C4-C3	178.7(5)	178.7(7)	179.6(8)	179.3(5)	179.4(5)/177.8(5)	–
average Pt-C$_{sp}$-C$_{sp}$	178.3	178.6	177.1	176.3	178.0	176.2
average C$_{sp}$-C$_{sp}$-C$_{sp}$	178.7	178.7	178.4	177.7	178.4	177.5
average sp/sp^3 distance[g]	–	–	4.865	4.034	4.422	–
average π stacking[h]	3.665	–	3.631	3.705	4.197	3.981
P-Pt-P/Pt angle[i]	0	0	0	0	189.3	41.0
Pt+P+P+C$_i$+C1 angle[i]	0	0	0	0	190.0	40.8

[a] This complex exhibits an inversion center at the midpoint of the PtC$_6$Pt chain. [b] Pt1−C1 and Pt2−C4; [c] C1−C2 and C3−C4. [d] C2−C3. [e] Pt1-C1-C2 and Pt2-C4-C3. [f] C1-C2-C3 and C4-C3-C2. [g] Average distance from every CH$_2$ group to the Pt−Pt vector. [h] Distance between midpoints of the C$_6$F$_5$ and C$_6$H$_4$R rings. [i] Angle between planes defined by these atoms on each endgroup.

driven self-assembly would occur to give molecules with the connectivities **A/B** (Scheme 1), analogously to earlier results with **PtC$_8$Pt**,[13] and 2) steric interactions that would raise

the energies of conformations with coplanar endgroups might still somehow result.
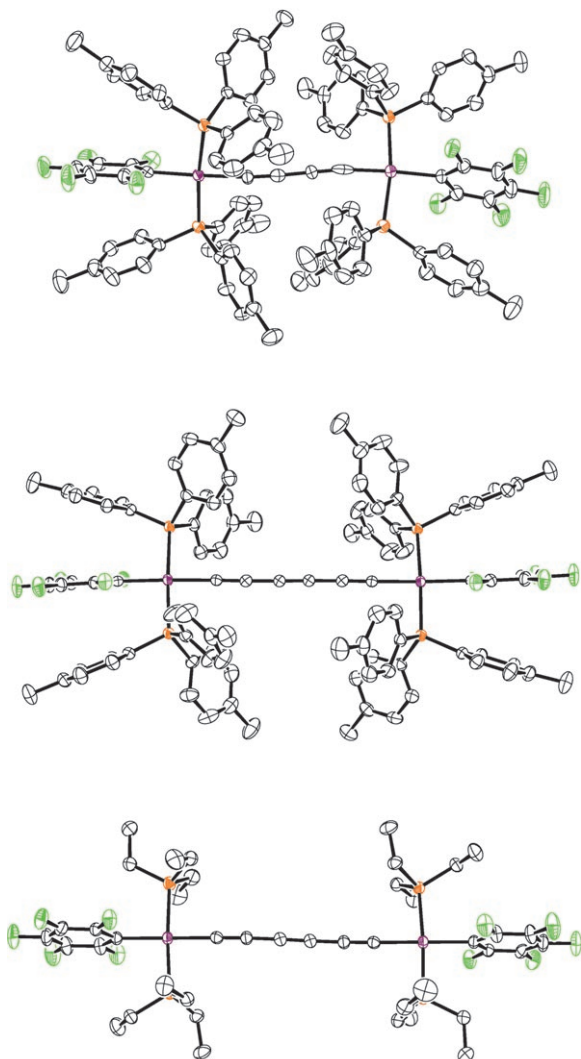
Figure 1. Thermal ellipsoid plots (50 % probability level) of **PtC₄Pt** (top), **PtC₆Pt·**4THF (middle; solvate molecules omitted), and **Pt′C₆Pt′** (bottom) (ellipsoids: purple = platinum, orange = phosphorus, green = fluorine, gray = carbon).
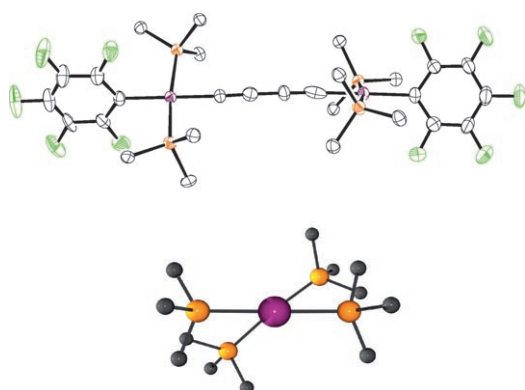

Figure 2. Partial views of the molecular structure of **PtC₄Pt** (ellipsoids/ spheres: purple = platinum, orange = phosphorus, green = fluorine, gray = carbon).
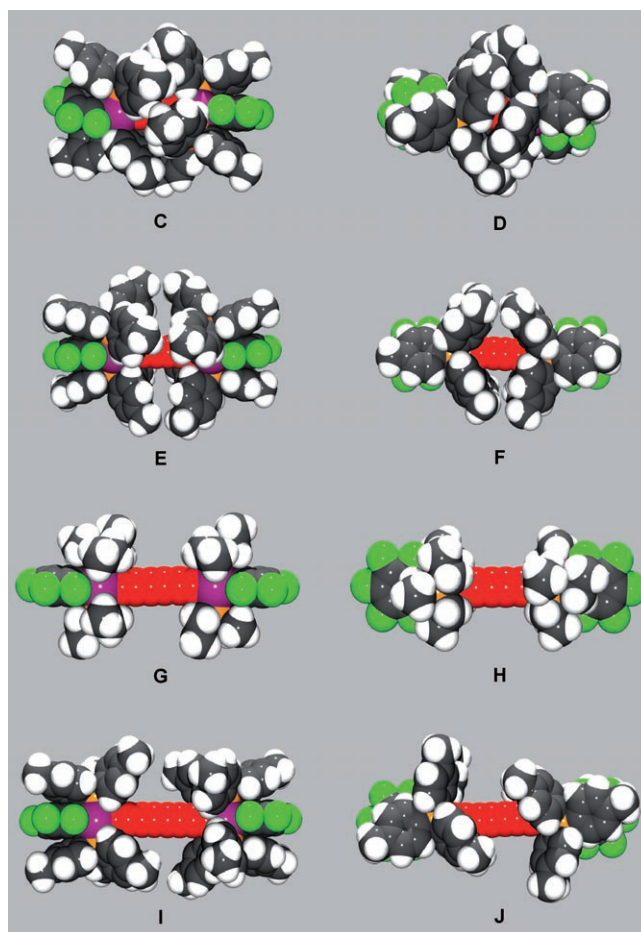

Figure 3. Space filling representations of **PtC₄Pt** (top), **PtC₆Pt·**4THF (second row), **Pt′C₆Pt′** (third row), and **PtC₈Pt** (bottom) parallel (left) and perpendicular (right) to the planes of the C_6F_5 ligands with solvate molecules omitted (spheres: purple = platinum, orange = phosphorus, green = fluorine, red = sp carbon chain).

As summarized in Scheme 3 (top), solutions of **PtC₆Pt** in THF were treated with a series of diphosphines Ar_2P-$(CH_2)_mPAr_2$ (m/Ar = 8/p-tol, 10/Ph, 11/Ph, 12/Ph, 14/p-tol, 14/p-C_6H_4-tBu, 16/Ph, 18/Ph).[28,29] In each case, the target complexes with endgroup-spanning diphosphines, *trans,-trans*-[(C_6F_5){($Ar_2P(CH_2)_mPAr_2$)}Pt(C≡C)₃Pt{($Ar_2P(CH_2)_m$P-Ar_2)}(C_6F_5)] (**PtC₆Pt-m/Ar**), formed. For the first six reactions, workups gave **PtC₆Pt-m/Ar** as light yellow solids in 57–82 % yields. For the last two, ³¹P NMR spectra of the reaction mixtures suggested complete conversion to **PtC₆Pt-16/Ph** and **PtC₆Pt-18/Ph**. However, the solids isolated (64 % in the former case) would not dissolve again. This is characteristic of oligomers that sometimes form upon sample concentration.[30] Similar behavior is seen if **PtC₈Pt** is combined with diphosphines with m ≥ 16, or **PtC₁₂Pt** with diphosphines with m ≥ 19.[13]

As noted with other complexes of the type **PtC$_x$Pt-m/ Ar**,[13–15] the mass spectra of **PtC₆Pt-m/Ar** exhibited intense molecular ions. The PtC≡CC ¹³C NMR spectroscopy signals of these diarylalkylphosphine adducts (PtC≡C, 95.7–
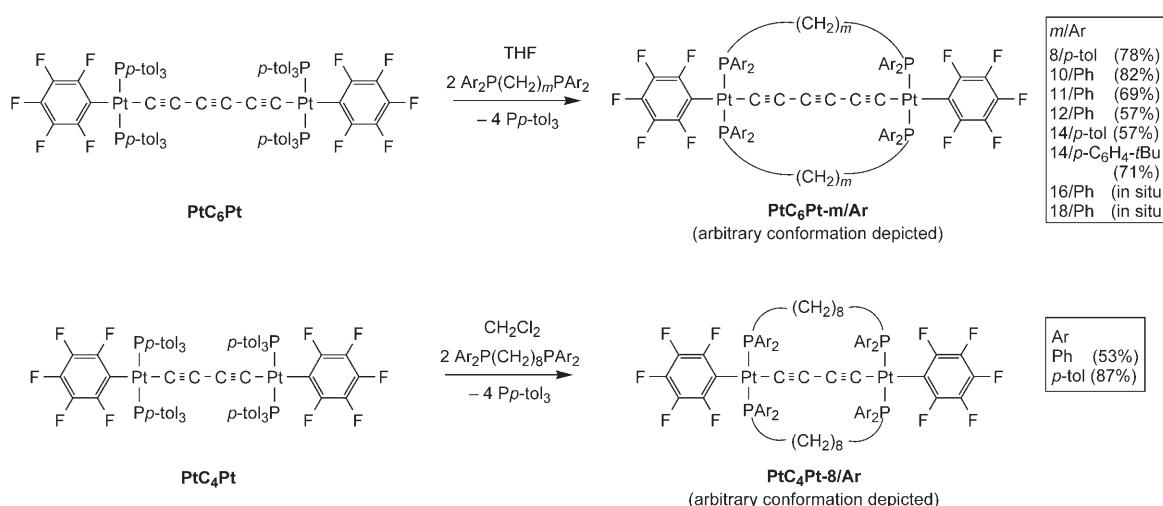
Scheme 3. Syntheses of diphosphine-bridged diplatinum hexatriynediyl and butadiynediyl complexes.

94.6 ppm; PtC≡CC, 61.7–60.3 ppm, CDCl₃) were very close to those of the triarylphosphine and trialkylphosphine models **PtC₆Pt** (95.8, 98.4, 61.1 ppm)[5] and **Pt'C₆Pt'** (91.7, 99.5, 60.2 ppm). The IR spectra showed a single weak $\tilde{\nu}_{C≡C}$ band (2100–2123 cm⁻¹), comparable to those of **PtC₆Pt** (2106 cm⁻¹) and **Pt'C₆Pt'** (2101 cm⁻¹). The UV/Visible spectra of representative complexes were recorded in CH₂Cl₂ [$\lambda(\varepsilon)$ = 313–323 (51 000–30 000), 345–343 (19 000–13 000), 370–368 nm (12 000–8000 M⁻¹cm⁻¹); see Experimental Section]. The band patterns were similar to that of **PtC₆Pt** ($\lambda(\varepsilon)$ = 315 (44 000), 345 (15 000), 358 (11 000), 369 nm (9000 M⁻¹cm⁻¹));[5] the underlying electronic transitions are analyzed in detail elsewhere.[9]

Structures of bridged hexatriynediyl complexes: The crystal structures of **PtC₆Pt-10/Ph**, **PtC₆Pt-11/Ph**, and **PtC₆Pt-14/p-tol**, or CH₂Cl₂ disolvates thereof, were determined. Most data are incorporated into Tables 1 and 2. Torsion angles associated with the sp³ chains are summarized in Table 3 and discussed below. Views of the molecular structures, the first two of which exhibit inversion centers at the midpoints of the sp chains and coplanar endgroups, are presented in Figure 4 and Figure 5. Two methylene groups of **PtC₆Pt-14/p-tol** are disordered (79:21 and 46:54 occupancy ratios), and only the dominant conformation is depicted.

The sp³ chains in **PtC₆Pt-10/Ph** are not long enough to twist into the double-helical conformation **A** (Scheme 1). Rather, a (CH₂)₇ segment in each (C3-

C9) runs roughly parallel to the sp chain in an "all-anti" conformation, laterally shielding two "sides" as in **B** (see Figure 4, top, or **K** in Figure 5). The sp³ chains in **PtC₆Pt-11/Ph** exhibit more curvature. Nonetheless, each returns to its hemisphere of origin (Figure 4, middle), avoiding a helical conformation.

The longer sp³ chains in **PtC₆Pt-14/p-tol** are able to wrap around the sp chain in a double-helical conformation **A**. The endgroups define an angle of 189.3°—more than a half twist. Both enantiomers are present in the unit cell. The sp chain is highly shielded, visible only through the bowl-like cavity highlighted in **P** in Figure 5. This view also reveals that the sp and sp³ chains are not in van der Waals contact. Interestingly, the average C₆H₄R/C₆F₅/C₆H₄R stacking distances are somewhat greater than in the other complexes (Table 2 and Figure 5; compare **O** with **K** and **M**). Additional features are analyzed below.

Table 3. Torsion angles [°] involving sp³ carbon atoms of Ar₂P(CH₂)ₘPAr₂-bridged complexes.[a]

	PtC₆Pt-10/Ph[b]	PtC₆Pt-11/Ph·2 CH₂Cl₂[b]	PtC₆Pt-14/p-tol·2 CH₂Cl₂[c]
Pt1-P1-C1-C2	176.0	40.0	60.3/37.9
P1-C1-C2-C3	152.0	177.5	−165.0/−156.7 (−89.0)
C1-C2-C3-C4	55.2	−179.0	−57.9/69.1 (−67.3)
C2-C3-C4-C5	58.9	59.4	−63.3/170.3 (−119.6)
C3-C4-C5-C6	167.4	54.2	−179.7/167.2 (−136.3)
C4-C5-C6-C7	165.8	59.8	174.1/78.0
C5-C6-C7-C8	170.1	175.2	64.3/164.8 (−158.4)
C6-C7-C8-C9	163.9	177.6	179.0/177.6 (−79.7)
C7-C8-C9-C10	−79.4	−173.5	174.6/−145.7 (166.2)
C8-C9-C10-P2 (-C11)[d]	168.6	75.2	−171.5/34.5 (−55.0)
C9-C10-P2-Pt2 (-C11-P2, -C11-C12)[d]	−179.0	−165.8	−64.3/−175.8
C10-C11-P2-Pt2 (-C12-C13)[d]	–	41.3	−55.8/176.5
C11-C12-C13-C14	–	–	−56.5/70.4
C12-C13-C14-P2	–	–	−169.2/−174.4
C13-C14-P2-Pt2	–	–	43.2/56.9

[a] The carbon atoms are numbered consecutively beginning at one terminus. [b] As this molecule exhibits an inversion center at the midpoint of the PtC₆Pt chain, the two sp³ chains are symmetry equivalent. [c] The sp³ chains in this molecule are not equivalent. The torsion angles for both are presented starting from the same platinum atom. The values in parentheses correspond to disordered segments and represent the minor conformer. [d] The first four atoms indicate the torsion angle for the first entry, and the atoms in parentheses indicate replacements for subsequent entries.
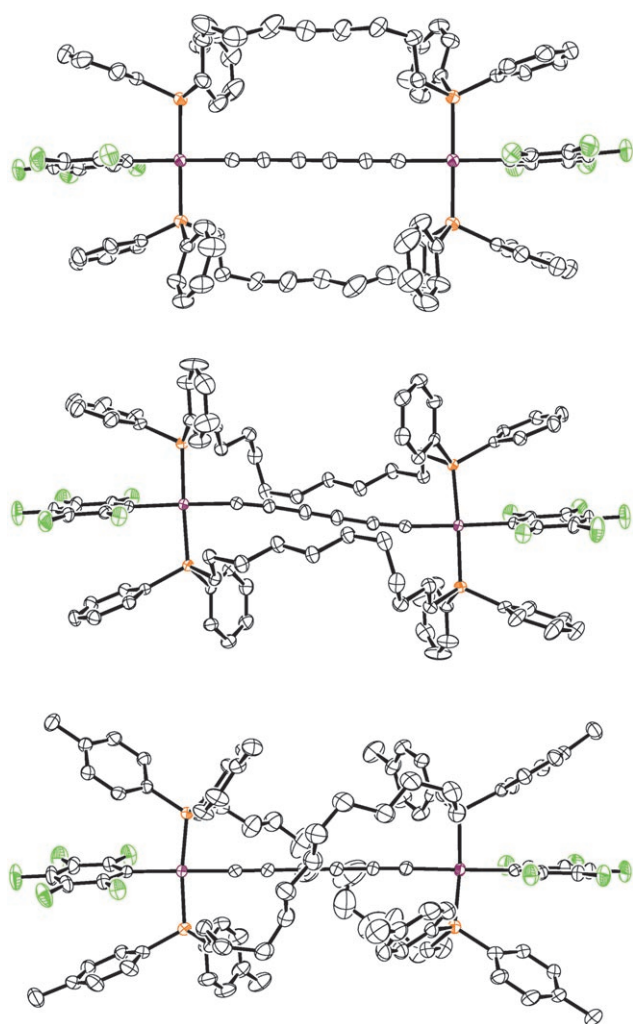
Figure 4. Thermal ellipsoid plots (50 % probability level) of **PtC₆Pt-10/Ph** (top), **PtC₆Pt-11/Ph**·2 CH₂Cl₂ (middle), and **PtC₆Pt-14/p-tol**·2 CH₂Cl₂ (bottom) with solvate molecules omitted (ellipsoids: purple = platinum, orange = phosphorus, green = fluorine, gray = carbon).

Figure 5. Space filling representations of **PtC₆Pt-10/Ph** (top), **PtC₆Pt-11/Ph**·2 CH₂Cl₂ (middle), and **PtC₆Pt-14/p-tol**·2 CH₂Cl₂ (bottom) parallel (left) and perpendicular (right) to the planes of the C_6F_5 ligands with solvate molecules omitted (spheres: purple = platinum, orange = phosphorus, green = fluorine, red = sp carbon chain).

The structure of **PtC₆Pt-14/p-tol** was probed in solution. As noted above, the aryl groups and PCH₂ protons are diastereotopic in the helical conformation **A**. However, when NMR spectra were recorded in CDClF₂ at −135 °C,[31] only a single set of aryl ¹³C or PCH₂ ¹H signals were observed. In connection with another structural issue below, ³¹P NMR spectra were recorded in [D₈]THF at low temperature. Although the signal broadened at −110 °C, no decoalescence occurred.

Syntheses and structures of bridged butadiynediyl complexes: Similar reactions of the butadiynediyl complex **PtC₄Pt** and the diphosphines Ar₂P(CH₂)₈PAr₂ (Ar = Ph, p-tol)[28,29] were investigated. As shown in Scheme 3 (bottom), workups gave the target complexes **PtC₄Pt-8/Ph** and **PtC₄Pt-8/p-tol** in good yields. However, the purifications were more difficult. With the former, chromatography was required. With the latter, small amounts of unidentified by-
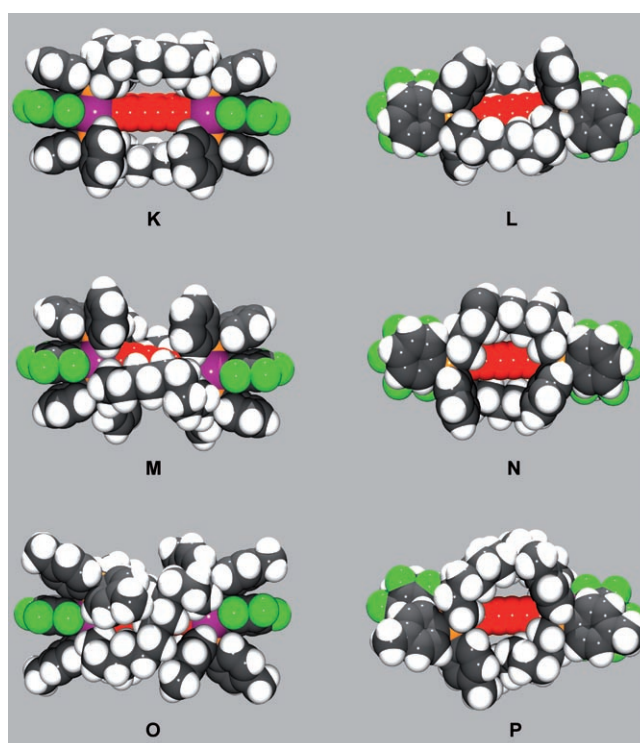
products could not be removed. The yield represents material of ≈ 97 % spectroscopic purity.

Given the non-coplanar endgroups in **PtC₄Pt**, it was hoped that the barriers for interconverting enantiomeric double-helical conformations of **PtC₄Pt-8/Ar** would be higher. Thus, ¹H, ¹³C, and ³¹P NMR spectra of both complexes were recorded at low temperature. To our initial delight, ¹H NMR spectra exhibited two signals for the PCH₂ protons at 193 K and below. The decoalescence of aryl protons was also apparent. With **PtC₄Pt-8/p-tol**, two methyl signals were also observed.

However, as depicted for **PtC₄Pt-8/Ph** in Figure 6, low-temperature ³¹P NMR spectra also exhibited *two* signals. The phosphorus atoms in the helical conformation **A** are homotopic (exchangeable by the three orthogonal C₂ axes) and should give only *one* signal. Alternative conformations consistent with these data are proposed in the discussion section. Key ³¹P NMR data for both complexes are summarized in Table 4. Standard protocols gave the simulation at the bottom of Figure 6, and $\Delta G^{\ddagger}$ values of 7.8–8.0 kcal mol⁻¹ or 32.6–33.6 kJ mol⁻¹ for the process that renders the phosphorus atoms equivalent.[33]

Thermal and oxidative stabilities: When the products in Scheme 3 were heated in capillaries, no melting was observed. Rather, solid-state decomposition (darkening) occurred at temperatures ranging from 160 to 255 °C. The
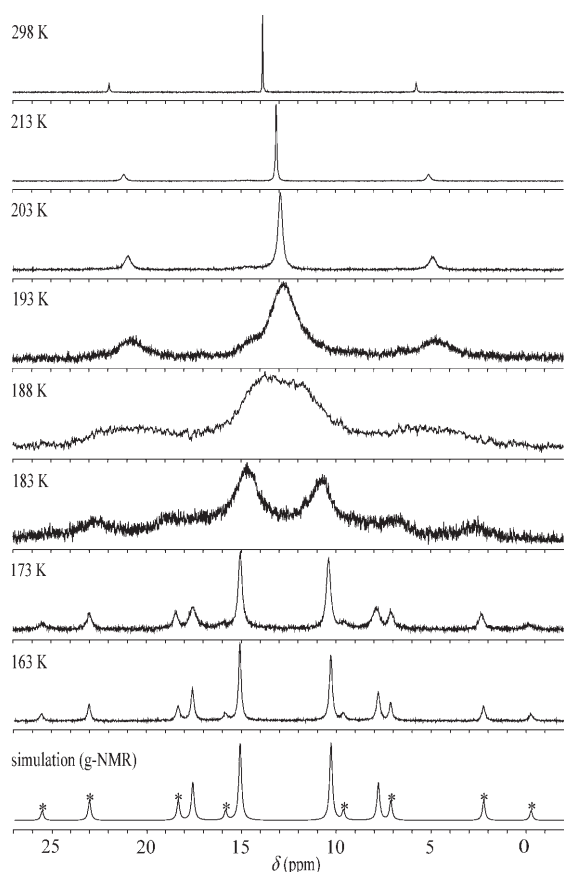
Figure 6. Variable-temperature $^{31}P\{^1H\}$ NMR spectra of **PtC₄Pt-8/Ph** (162 MHz, [D₈]THF; * denotes a platinum satellite).

Table 4. Key $^{31}P\{^1H\}$ NMR data for **PtC₄Pt-8/Ph** (Figure 6) and **PtC₄Pt-8/p-tol** (162 MHz, [D₈]THF, *AB* spin systems).

	PtC₄Pt-8/Ph	**PtC₄Pt-8/p-tol**
P_A (σ, 163 K)	16.16 ppm	14.75 ppm
P_B (σ, 163 K)	9.32 ppm	7.96 ppm
$\Delta\nu$ (163 K)	1108.9 Hz	1098.2 Hz
$|J_{AB}|$ (163 K)	404.0 Hz	405.7 Hz
T_C	188 K	193 K
k_C	3302 s⁻¹	3290 s⁻¹
$\Delta G^{\ddagger}(T_C)$	32.6 kJ mol⁻¹	33.6 kJ mol⁻¹
	7.8 kcal mol⁻¹	8.0 kcal mol⁻¹

hexatriynediyl complexes **PtC₆Pt-8/p-tol**, **PtC₆Pt-10/Ph**, **PtC₆Pt-12/Ph** and **PtC₆Pt-14/p-tol** were further characterized by TGA and DSC. There was no appreciable mass loss below 270 °C. Endotherms were observed at 291, 214, 225, and 165 °C (T_e),[34] respectively, roughly paralleling the capillary behavior. The preceding observations suggest that the stabilities decrease with increasing sp³ chain length.

All of the diplatinum complexes were stable for extended periods in air. As summarized in Table 5, cyclic voltammograms of representative adducts were recorded under conditions employed for related complexes earlier.[5,6,11–15] Partially reversible oxidations were observed, as reflected by the $i_{c/a}$ and ΔE values. Mixed-valent platinum(II)/platinum(III)

Table 5. Cyclic voltammetry data.

Complex[a]	$E_{p,a}$ [V]	$E_{p,c}$ [V]	$E°$ [V]	ΔE [mV]	$i_{c/a}$
PtC₄Pt	0.940	0.862	0.901	78	0.98
PtC₄Pt-8/Ph	1.054	0.976	1.015	78	0.94
PtC₆Pt	1.156	1.066	1.111	90	0.71
PtC₆Pt-10/Ph	1.245	1.160	1.203	85	0.82
PtC₆Pt-12/Ph	1.225	1.150	1.188	75	0.84
PtC₆Pt-14/p-tol	1.238	1.121	1.180	117	0.45

[a] Conditions: 22.5 ± 1 °C, CH₂Cl₂ solutions (7–9) × 10⁻⁵ M in complex and 0.1 M in nBu₄N⁺ BF₄⁻; Pt working and counter electrodes, potential vs. Ag wire pseudoreference; scan rate, 100 mV s⁻¹; ferrocene = 0.46 V.

radical cations were presumed to form.[35] The unbridged complexes **PtC$_x$Pt** exhibited thermodynamically more favorable oxidations (less positive $E°$ values) with shorter sp chain lengths, which parallel the HOMO energies, as analyzed in detail previously.[5,9] Concurrently, the reversibilities improved.

When the Pp-tol₃ ligands in **PtC₄Pt** were replaced by the diphenylalkylphosphine ligands in **PtC₄Pt-8/Ph**, oxidations became thermodynamically less favorable. The higher homologues **PtC₆Pt/PtC₆Pt-m/Ph** (Table 5) and **PtC₈Pt/PtC₈Pt-m/Ph**[13,14] behaved similarly. With **PtC₄Pt** and **PtC₄Pt-8/Ph**, the reversibilities were comparably high. In contrast, the bridged complexes **PtC₆Pt-10/Ph** and **PtC₆Pt-12/Ph** gave somewhat more reversible oxidations than **PtC₆Pt**. Unexpectedly, **PtC₆Pt-14/p-tol** exhibited a much less reversible oxidation—the first time such a trend has been found for a complex that can adopt helical conformation **A**. Platinum(III) species can decompose by means of solvent interaction with an axial coordination site.[35] However, as illustrated by **O** and **K** in Figure 5, the axial sites in **PtC₆Pt-14/p-tol** are much more sterically shielded than those in **PtC₆Pt-10/Ph**. Perhaps the larger ring size in **PtC₆Pt-14/p-tol** labilizes the resulting radical cation.

Discussion

Syntheses: The new syntheses in Scheme 3 parallel those reported earlier for the bridged octatetraynediyl complexes **PtC₈Pt-m/Ar** (m = 10, 11, 12, 14) and dodecahexaynediyl complex **PtC₁₂Pt-18/Ph**.[13] Thus, this approach to sterically shield the unsaturated assemblies that connect two electroactive groups has considerable generality. Efforts by other researchers have largely focused on various types of dendrimers or rotaxanes.[16] These often contain reactive functional groups, whereas our assemblies are encased by the equivalent of polyethylene. The protocol in Scheme 3 can be regarded as a one-dimensional analog of the coordination-driven self-assembly processes used by Stang and Fujita to access two- and three-dimensional polypalladium and polyplatinum complexes with other types of rigid spacers.[36]

For an sp chain of x carbon atoms, there must be a minimum sp³ chain length of m carbon atoms. The data for **PtC₆Pt** (Scheme 3) and **PtC₈Pt**[13] establish that m can be as little as $x+2$. For such species, conformations of the type **B**

are clearly the only energetically reasonable possibilities. There also seems to be an upper limit on the sp³ chain length, at least from an operational standpoint. In the case of **PtC₁₂Pt**, essentially, only oligomers can be isolated if the sp³ chain is >50% longer than the sp chain ($m > 18$). With **PtC₈Pt**, the corresponding limit is >75% ($m > 14$). With **PtC₆Pt**, the practical limit appears to be >133% ($m > 14$), although higher homologues ($m = 16, 18$) clearly form in situ. With **PtC₄Pt**, the sp³ chains can be 200% longer than the sp chain. However, given the non-coplanar endgroups and different conformational motif of the products, we view results in this series (where the sp³ chain length has not yet been varied) as less comparable.

The other synthetic approach to bridged complexes **PtCₓPt-m/Ar** in Scheme 1 – the metathesis/hydrogenation sequence – has so far only been applied to complexes with $x = 8$ and 12. Although overall yields are lower, it is a more reliable protocol for these sp chain lengths. Importantly, it has proved possible to isolate **PtC₈Pt-16/Ph**, **PtC₈Pt-18/Ph**, **PtC₈Pt-20/Ph**, **PtC₁₂Pt-18/Ph**, and **PtC₁₂Pt-20/Ph**—all of which are inaccessible from **PtCₓPt** and the corresponding diphosphines. Thus, these complexes are not intrinsically unstable towards oligomerization. It therefore remains possible that **PtC₆Pt-16/Ph** and **PtC₆Pt-18/Ph**, which similarly decompose under the workup conditions in Scheme 3, are isolable molecules. Perhaps oligomerization is promoted by some component of the reaction mixture, such as the displaced P*p*-tol₃ or any excess Ar₂P(CH₂)ₘPAr₂.

Structures of bridged hexatriynediyl complexes: The three structurally characterized bridged hexatriynediyl complexes **PtC₆Pt-m/Ar** (Figure 4, 5) are best analyzed with reference to octatetraynediyl analogs **PtC₈Pt-m/Ar**,[13–15] key data for which are summarized in Table 6. The latter crystallize in non-helical conformations **B** when $m = 10$ or 12 (Ar=Ph), and double-helical conformations **A** when $m = 14$ (Ar=Ph, *p*-tol, *p*-C₆H₄-*t*Bu) and 20 (Ar=Ph). When $m = 10$–14, the endgroups are approximately coplanar. The angles defined by the P-Pt-P/Pt planes in the helical species **PtC₈Pt-14/Ar**

range from 189.9° to 196.6°—slightly more than a half twist. However, this angle significantly increases in the complex with the longest sp³ chain, **PtC₈Pt-20/Ph**, reaching 294.8°, or more than three-quarters of a twist.

As summarized in Table 2, the hexatriynediyl complexes **PtC₆Pt-m/Ar** also crystallize with coplanar or nearly coplanar endgroups. Like the octatetraynediyl complexes, non-helical conformations **B** are found with lower values of m (10, 11), and helical conformations **A** with higher values (14). In the last case, the helix defines slightly more than a half twist (P-Pt-P/Pt angle, 189.3°). Computational studies of non-bridged model compounds do not reveal any electronic driving force for coplanar endgroups.[9] Hence, their preponderance in the crystal structures might reflect some deepseated lattice packing preference.

For both helical and non-helical complexes, the average distance of the sp³ carbon atoms from the platinum-platinum vector can be calculated. The values (Tables 2 and 6) approximate the average sp³/sp distances. Those for the non-helical octatetraynediyl complexes **PtC₈Pt-10/Ph** and **PtC₈Pt-12/Ph** and helical analogs **PtC₈Pt-14/Ar** are similar (3.932–4.090 vs. 3.977–4.053 Å), and slightly greater than the sum of the van der Waals radii (3.48, or 1.78/1.70 Å sp/sp³).[32] When hydrogen atoms are included (van der Waals radius 1.20 Å), space-filling models show significant numbers of van der Waals contacts. A larger average sp/sp³ distance indicates a "looser" helix with a greater radius, which should in turn have fewer van der Waals contacts. Furthermore, as the sp³ chains become longer, the contact surface of the sp chain will eventually be saturated, requiring either helices of greater radii or alternative conformations. Accordingly, the average sp/sp³ distance in **PtC₈Pt-20/Ph** increases to 4.133 Å.

Upon going from octatetraynediyl to hexatriynediyl complexes, the contact surface of the sp chain decreases. Thus, the helical hexatriynediyl complex **PtC₆Pt-14/p-tol** exhibits a much greater average sp/sp³ distance than octatetraynediyl homologues with identical sp³ chain lengths (**PtC₈Pt-14/Ar**; 4.422 vs. 3.977–4.053 Å). As shown in **P** in Figure 5, van der

Table 6. Key crystallographic data for bridged octatetraynediyl complexes **PtC₈Pt-m/Ar**.

Complex[13–15]	Conformation[a]	P-Pt-P/Pt plane/ plane angle [°][b]	Average sp/sp³ distance [Å][b]	Anti/gauche PAr₂CH₂CH₂CH₂, CH₂CH₂CH₂CH₂[c]	
				sp³ chain #1	sp³ chain #2
PtC₈Pt-10/Ph·(toluene)₄	**B**	0.2	3.932	8/1 (1:0)	disorder[d]
PtC₈Pt-10/Ph·(CHCl₃)₂	**B**	5.1	3.989	8/1 (1:0)	8/1 (1:0)
PtC₈Pt-12/Ph·(CH₂Cl₂)₂.₅	**B**	12.9	4.090	8/3 (2:1)	disorder[d]
PtC₈Pt-14/Ph·(benzene)₁.₅	**A**	196.6	4.053	9/4 (4:0)	9/4 (2:2)
PtC₈Pt-14/Ph·(toluene)₁.₅	**A**	196.5	3.977	9/4 (4:0)	10/3 (3:0)
PtC₈Pt-14/p-tol	**A**	189.9	4.042	10/3 (3:0)	9/4 (4:0)
PtC₈Pt-14/p-C₆H₄-tBu·(toluene)₅.₅[e]	**A**	193.3	3.988	9/4 (4:0)	9/4 (4:0)
PtC₈Pt-20/Ph	**A**	294.8	4.133	12/7 (5:2)	disorder[d]
PtC₈Pt-16/Ph·MeOH[f]	**A**	164.1	4.279	9/6 (4:2)	8/7 (4:3)

[a] See Scheme 1. [b] See Table 2 for definitions. [c] Segments with torsion angles between +30° and +90° or −30° and −90° are considered gauche; the ratio of positive/negative gauche torsion angles is given in parentheses (arbitrary direction, as the ratio inverts for the enantiomer). [d] No attempt is made to analyze disordered sp³ chains, although all torsion angles can be found in the original publications.[13–15] [e] Analogous data for the pseudopolymorph **PtC₈Pt-14/p-C₆H₄-tBu**·(toluene)₂ with conformation **A**: 0.0°, 4.064 Å, 8/5 (4:1), 8/5 (4:1). [f] The sp³ chain in this complex consists of two oxygen atoms and fourteen CH₂ groups.

Waals contacts are dramatically diminished. The average sp/sp^3 distance in non-helical **PtC$_6$Pt-11/Ph** (4.034 Å) falls within the range of the octatetraynediyl complexes. However, that in **PtC$_6$Pt-10/Ph** (4.865 Å) is the longest found for a **PtC$_x$Pt-m/Ar** species to date. The enhanced spacing is easily seen in **K** in Figure 5. Curiously, **PtC$_6$Pt-10/Ph** is the only complex in which all of the PtPAr$_2$CH$_2$CH$_2$ segments exhibit *anti* conformations, as indicated by the torsion angles in Table 3.[37] This extends the PCH$_2$CH$_2$ carbon atoms as far from the sp chain as possible.

As highlighted in Figure 7 (top), gauche segments (torsion angles between $+30°$ and $+90°$ or $-30°$ and $-90°$) are chiral. Although the bridged polyynediyl complexes feature
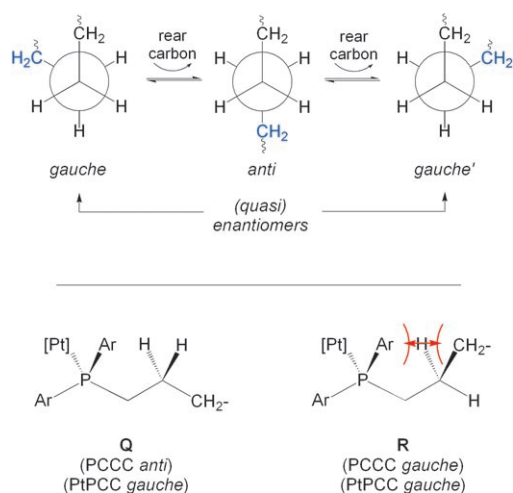

Figure 7. Some conformational issues in double-helical complexes **A**. An important step in enantiomer interconversion (top). Steric interactions as a function of PAr$_2$CH$_2$CH$_2$CH$_2$ conformations (bottom).

other types of stereogenic units, the helical chirality is primarily derived from the gauche segments associated with the sp^3 chains. A number of patterns are evident in the torsion angles (Table 3 and Tables in earlier papers).[13–15] First, despite the conformation of **PtC$_6$Pt-10/Ph**, the PtPAr$_2$CH$_2$CH$_2$ segments are nearly always gauche.[37] Second, the PAr$_2$CH$_2$CH$_2$CH$_2$ segments are nearly always anti. This avoids 1,5-synperiplanar interactions[38] involving the PAr$_2$ groups as illustrated in Figure 7 (bottom). Third, the neighboring CH$_2$CH$_2$CH$_2$CH$_2$ segments are nearly always gauche, with the one exception in Table 3 involving **PtC$_6$Pt-11/Ph**.

Consider the PAr$_2$CH$_2$CH$_2$CH$_2$ and CH$_2$CH$_2$CH$_2$CH$_2$ segments of the non-disordered sp^3 chain in **PtC$_6$Pt-14/p-tol**. Six are gauche (Table 3), as compared to three-four in the four octatetraynediyl homologues **PtC$_8$Pt-14/Ar** (Table 6). Thus, it is intrinsically more kinked. Furthermore, the gauche segments in each sp^3 chain of **PtC$_8$Pt-14/Ar** exhibit, with a single exception, the same sign or handedness. However, the non-disordered chain in **PtC$_6$Pt-14/p-tol** features five gauche segments of one sign, and one of the other. The situation with the helical octatetraynediyl complex with the

longest sp^3 chain, **PtC$_8$Pt-20/Ph**, is similar (five gauche segments of one sign, two of the other). The complex designated as **PtC$_8$Pt-16/Ph** in Table 6, in which the phosphorus atoms are spanned by fourteen methylene groups and two oxygen atoms, also shares many of these properties.

We rationalize these trends as follows. If the endgroups twist to the maximum degree allowed by the sp^3 chain lengths, all gauche segments should have the same sign or helical chirality. The octatetraynediyl complexes **PtC$_8$Pt-14/Ar** are better able to approach this limit than **PtC$_6$Pt-14/p-tol**, as the (CH$_2$)$_{14}$ chains span a greater distance. Thus, there is more "play" in the sp^3 chains of **PtC$_6$Pt-14/p-tol**, as reflected by the greater average sp^3/sp chain distance. Furthermore, if there are too many gauche segments of the same handedness, the sp^3 chains would "overshoot" the plane of the second endgroup, and would need to "double back" by means of gauche segments of the opposite handedness. This "correction" occurs in the middle of the non-disordered chain of **PtC$_6$Pt-14/p-tol** (C5-C6-C7-C8). For both **PtC$_6$Pt-14/p-tol** and **PtC$_8$Pt-20/Ph**, this phenomenon is easily tracked on computer screens with standard visualization programs.

Structures of bridged butadiynediyl complexes: Formally, the generation of bridged derivatives of **PtC$_4$Pt** involves the removal of four aryl groups and the introduction of two sp^3 chains. However, as is evident from views **C** and **D** of crystalline **PtC$_4$Pt** (Figure 3), removing the aryl groups makes only a modest amount of sp contact surface available. Therefore, it is questionable whether a butadiynediyl core can support double-helical conformations **A**. Nonetheless, the fact that **PtC$_4$Pt-8/Ph** and **PtC$_4$Pt-8/p-tol** exhibit two ^{31}P NMR signals at low temperature (Figure 6 and Table 4) requires ground state conformations of lower symmetry than **B** (point group D_{2h}).

Consider the starting structures **S** and **T** of C_{2h} and C_{2v} symmetry in Figure 8. These have coplanar endgroups—which renders them improbable ground state conformations—and hence eclipsed P-Pt-P linkages. Each phosphorus-carbon bond is also eclipsed with a phosphorus-carbon bond of the *syn* phosphorus atom on the opposite platinum (blue/blue or red/red). The sp^3 chains bridge two eclipsed positions. In **S**, the sp^3 chains are on opposite sides of the endgroup planes (*anti*), and in **T** they are on the same sides (*syn*). Although no aryl rings are depicted, note that the aryl/C$_6$F$_5$/aryl stacking interactions can be maintained (these would involve aryl groups in the wedged positions extending in front and behind the plane of the paper).

Next consider the new conformations **U** and **V** generated by rotating the planes of the front endgroups counterclockwise and rear endgroups clockwise. These are chiral and of C_2 symmetry. The former, which retains an *anti* sense, exhibits a C_2 axis along the sp chain. The latter, which retains a *syn* sense, exhibits a C_2 axis perpendicular to the midpoint of the sp chain. In both cases, aryl/C$_6$F$_5$/aryl stacking interactions can be maintained (again involving wedged positions in front and behind the plane of the paper).
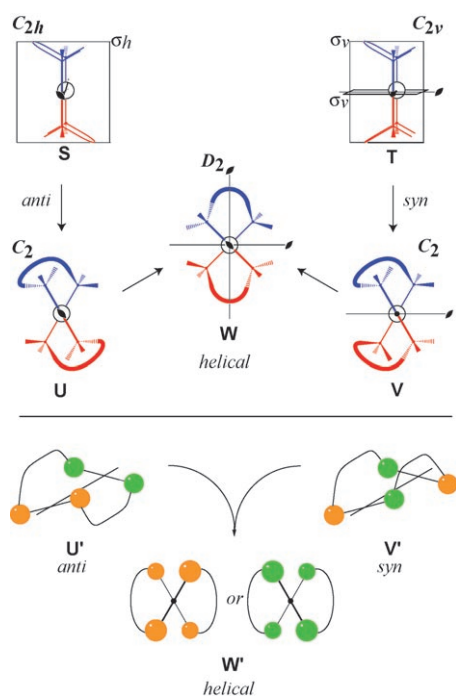
Figure 8. Selected limiting conformations for **PtC₄Pt-8/Ar**.

One way to interconvert **U** and **V** would involve continued endgroup rotation to the originally targeted chiral helical conformation **W** (D_2 symmetry). This requires significant platinum-phosphorus bond rotation and disruption of the aryl/C_6F_5/aryl stacking interactions, as the participating PAr_2 groups must be exchanged. There are additional possible equilibria, as well as more exotic candidates for conformational ground states, as diagrammed elsewhere.[24] However, the NMR data in Figure 6 and Table 4 are analyzed with respect to the limiting conformations in Figure 8, which feature little if any contact between the sp and sp^3 chains.

Alternative representations of **U**, **V**, and **W** are depicted at the bottom of Figure 8 (**U′**, **V′**, **W′**). In the latter set, phosphorus atoms that are homotopic are assigned identical colors (orange or green). The two orange phosphorus atoms in the chiral C_2 conformations **U** and **V** can be exchanged by C_2 axes, as can the two green phosphorus atoms. However, the orange and green atoms are diastereotopic, and should give separate ^{31}P NMR signals ($AA'BB'$ spin systems). As already noted for **A** above, all phosphorus atoms in D_2 helical conformations are homotopic, and should give only one ^{31}P NMR signal. For similar reasons, **S** and **T** (and **B**) should give one ^{31}P NMR signal (all phosphorus atoms homotopic or enantiotopic).

Do any of the NMR spectroscopic data allow **U** and **V** to be distinguished? Note that in **V**, the phosphorus atoms on each termini are diastereotopic, and significant coupling would be expected. In contrast, in **U** the phosphorus atoms on each termini are homotopic; the diastereotopic phosphorus atoms occupy the other terminus. Therefore, a much smaller coupling would be expected. Hence, given the large

404–406 Hz couplings (Figure 6 and Table 4), **PtC₄Pt-8/Ph** and **PtC₄Pt-8/p-tol** are proposed to have the *syn* ground state conformations **V**.[39] The dynamic process that renders the phosphorus atoms formally equivalent might involve an equilibrium with **T**, followed by endgroup twisting in the opposite direction, or an equilibrium with **W**.

Conclusion and Perspective

We have been able to extend coordination-driven self-assembly reactions developed earlier for bridged diplatinum octatetraynediyl and dodecahexaynediyl complexes[13,15] to hexatriynediyl and butadiynediyl complexes **PtCₓPt-m/Ar** (Scheme 3). In accord with previous results, systems with longer sp^3 chains show a greater tendency towards oligomerization. However, numerous adducts can be isolated and in many cases structurally characterized.

The crystal structures of the bridged hexatriynediyl complexes exhibit, depending upon the lengths of the sp^3 chains, either idealized chiral helical conformations **A** ($m = 14$) or formally achiral conformations **B** ($m = 10, 11$). It was hoped that endgroup/endgroup interactions might destabilize **B** relative to **A**, facilitating the definitive observation of **A** by NMR in solution. However, model compounds lacking the sp^3 chains did not exhibit van der Waals contacts.

Therefore, butadiynediyl complexes with still shorter sp chains were investigated. Now the endgroups of model complexes lacking the sp^3 chains showed marked van der Waals contacts, resulting in plane/plane angles of $\approx 40°$. However, the sp chain becomes nearly completely shielded, with little contact surface to support helical sp^3 chains. Hence, alternative conformations are necessary, and low-temperature NMR data ($m = 8$) are best modeled by a twisted chiral conformation in which both sp^3 chains bow in a *syn* manner, unlike the in-plane bow implied in **B**.[39]

In order for **A** to interconvert with enantiomer **A′**, each chiral gauche segment in the sp^3 chain must invert. The activation barrier for the conversion of gauche to anti butane is ≈ 2.7 kcal mol^{-1}. If the rate determining step featured one such local transition state in each sp^3 chain, the barrier would be at least 5.4 kcal mol^{-1}. However, these barriers would in turn be derived from local minima lying appreciably above the ground state. Therefore, we continue to believe that it should be possible to render the equilibrium **A**/**A′** slow on the NMR timescale. Complexes in which the platinum endgroups are spaced by five sp carbon atoms would be ideal, but unfortunately this is not chemically feasible. Alternatively, with much longer sp/sp^3 chains, helical conformations might be stabilized by additional van der Waals and possibly CH/π interactions.

Other types of sterically shielded polyynediyl complexes, certain of which may be able to address some of these issues, remain under active investigation. These, together with architecturally new types of assemblies based upon Pt-(C≡C)$_n$Pt building blocks, will be described in future publications.[40]

Experimental Section

General: Reactions were conducted under N_2 atmospheres, and workups in air. Chemicals were used as follows: hexane and THF, distilled from Na/benzophenone; CH_2Cl_2, distilled from CaH_2; methanol and ethanol, distilled; $CDCl_3$, stored over molecular sieves; $CDFCl_2$, prepared by a literature procedure,[31] nBu_4N^+ F^- (trihydrate, Lancaster), dissolved in THF containing 5 wt% H_2O to give a 1.0 M solution; [D$_8$]THF (Aldrich), CuCl (Aldrich, 99.99%), tBuOK (Fluka), KPF$_6$ (Acros), and PEt$_3$ (Strem, 10 wt% in hexane), used as received. Instrumentation, and procedures for recording DSC/TGA[34] and cyclic voltammetry data, were identical to those in previous papers.[13–15]

All NMR spectra were recorded in at ambient temperature unless noted. The solvent was $CDCl_3$, except for the variable-temperature ^{31}P data measurements for which [D$_8$]THF was used. All NMR spectra were recorded on either 300 or 400 MHz spectrometers.

***trans,trans*-[(C$_6$F$_5$){(*p*-tol$_3$P)$_2$}Pt(C≡C)$_3$Pt{(P*p*-tol)$_3$)$_2$}(C$_6$F$_5$) (PtC$_6$Pt)**:[5] A Schlenk flask was charged with **PtC$_6$SiEt$_3$** (1.380 g, 1.194 mmol), degassed THF (150 mL), methanol (150 mL), and nBu_4N^+ F^- (0.24 mL, 1.0 M in THF/5 wt% H_2O, 0.24 mmol). The solution was stirred for 15 min, and then **PtCl** (1.200 g, 1.174 mmol), KPF$_6$ (0.240 g, 1.31 mmol), tBuOK (0.160 g, 1.43 mmol), and CuCl (0.096 g, 0.096 mmol) were added. After 16 h, the precipitate was collected by filtration, washed with methanol (2×30 mL), and air dried to give **PtC$_6$Pt** as a yellow powder (2.240 g, 1.112 mmol, 95% based upon **PtCl** (limiting reagent), or 93% based upon **PtC$_6$SiEt$_3$**). $^{31}P\{^1H\}$ NMR: $\delta = 17.8$ ppm (s, $^1J_{PPt} = 2684$ Hz);[41] IR (powder film): $\tilde{\nu} = 2106$ cm^{-1} (br m, C≡C).

***trans,trans*-[(C$_6$F$_5$){(Et$_3$P)$_2$}Pt(C≡C)$_3$Pt{(PEt$_3$)$_2$}(C$_6$F$_5$) (Pt′C$_6$Pt′)**: A Schlenk flask was charged with **PtC$_6$Pt** (0.200 g, 0.099 mmol), THF (40 mL), and PEt$_3$ (0.75 mL, 0.45 mmol, 10% wt in hexane). The mixture was stirred (3 h) and concentrated (to ≈5 mL). Hexane (30 mL) was added. The precipitate was collected by filtration, washed with ethanol (2×10 mL), and dried by oil pump vacuum to give **Pt′C$_6$Pt′** as a yellow solid (0.090 g, 0.071 mmol, 72%). ^1H NMR:[42] $\delta = 1.78$ (m, 24 H; PCH_2), 1.09 ppm (m, 36 H; PCH$_2$CH_3); $^{13}C\{^1H\}$ NMR: $\delta = 147$ (br dm, $^1J_{CF} = 218$ Hz, $^2J_{CF} = 22.2$ Hz, o to Pt), 136 (dm, $^1J_{CF} = 248$ Hz, p/m to Pt), 120.3 (virtual t, $^2J_{CF} = 121$ Hz, i to Pt), 99.5 (br s, PtC≡C),[43] 91.7 (s, PtC≡C, $^1J_{PtC} = 283$ Hz),[41] 60.2 (s, PtC≡CC, $^3J_{PtC} = 40$ Hz),[41] 16.0 (virtual t, $^1J_{CP} = 17.5$ Hz, $^2J_{PtC} = 70.7$ Hz),[41] PCH$_2$CH$_3$), 8.2 ppm (s, $^3J_{PtC} = 24.6$ Hz, PCH$_2$CH$_3$); $^{31}P\{^1H\}$ NMR: $\delta = 14.0$ ppm (s, $^1J_{PPt} = 2412$ Hz).[41] IR (powder film): $\tilde{\nu} = 2101$ cm^{-1} (m, C≡C); FAB-MS: m/z (%):[44] 1268 (100) [M]$^+$, 788 (85) [M−Pt−PEt$_3$−C$_6$F$_5$]$^+$; elemental analysis calcd (%) for C$_{42}$H$_{60}$F$_{10}$P$_4$Pt$_2$: C 39.75, H 4.77; found: C 39.85, 4.77.

***trans,trans*-[(C$_6$F$_5$){(*p*-tol$_2$P(CH$_2$)$_8$P*p*-tol$_2$)}Pt(C≡C)$_3$Pt{(*p*-tol$_2$P(CH$_2$)$_8$P*p*-tol$_2$)}(C$_6$F$_5$)] (PtC$_6$Pt-8/*p*-tol)**: A Schlenk flask was charged with **PtC$_6$Pt** (0.228 g, 0.113 mmol) and THF (75 mL). Solid *p*-tol$_2$P(CH$_2$)$_8$P*p*-tol$_2$ (0.144 g, 0.272 mmol)[29] was added in one portion with stirring. After 36 h, the mixture was concentrated (to ≈20 mL) and ethanol (50 mL) was added. The precipitate was collected by filtration, washed with ethanol (2×10 mL), and dried by oil pump vacuum to give **PtC$_6$Pt-8/*p*-tol** as a light yellow solid (0.165 g, 0.088 mmol, 78%), decomp point 255°C (capillary, gradual darkening without melting). DSC: endotherm: $T_i = 277.4$, $T_e = 291.3$, $T_p = 302.6$, $T_c = 309.4$, $T_f = 309.7$°C; TGA (onset of mass loss): $T_i = 298.3$, $T_e = 309.5$, $T_f = 400.4$°C; ^1H NMR:[42] $\delta = 7.27$ (m, 16 H; o to P), 7.03 (br d, $^3J_{HH} = 7.7$ Hz, 16 H; m to P), 2.72 (m, 8 H; PCH_2), 2.32 (s, 24 H; CH_3), 1.87 (m, 8 H; PCH$_2$CH_2), 1.49 (m, 8 H; PCH$_2$CH$_2$CH_2), 1.35 ppm (m, 8 H; PCH$_2$CH$_2$CH$_2$CH_2); $^{13}C\{^1H\}$ NMR: $\delta = 146$ (br m, o to Pt), 140.8 (s, p to Pt), 137 (br m, m/p to Pt), 133.4 (virtual t, $^2J_{CP} = 5.8$ Hz, o to P), 129.1 (virtual t, $^1J_{CP} = 28.2$ Hz, i to Pt), 128.9 (virtual t, $^3J_{CP} = 5.3$ Hz, m to P), 95.7 (s, PtC≡C),[43,45] 61.7 (s, PtC≡CC), 32.3 (virtual t, $^3J_{CP} = 7.3$ Hz, PCH$_2$CH$_2$), 29.7 (s, PCH$_2$CH$_2$CH$_2$), 27.8 (virtual t, $^1J_{CP} = 18.4$ Hz, PCH_2), 25.8 (s, PCH$_2$CH_2), 21.3 ppm (s, CH_3); $^{31}P\{^1H\}$ NMR: $\delta = 11.8$ ppm (s, $^1J_{PPt} = 2567$ Hz);[41] IR (powder film): $\tilde{\nu} = 2108$ cm^{-1} (br w, C≡C); UV/Vis (CH$_2$Cl$_2$, 1.25×10^{-5} M): $\lambda(\varepsilon) = 345$ (19000), 370 nm (12000 M^{-1} cm^{-1}); FAB-MS: m/z (%):[44] 1871 (100) [M−H]$^+$; elemental analysis calcd (%) for C$_{90}$H$_{88}$F$_{10}$P$_4$Pt$_2$: C 57.69, H 4.73; found: C 56.97, H 4.74.

***trans,trans*-[(C$_6$F$_5$){(Ph$_2$P(CH$_2$)$_{10}$PPh$_2$)}Pt(C≡C)$_3$Pt{(Ph$_2$P(CH$_2$)$_{10}$PPh$_2$)}(C$_6$F$_5$)] (PtC$_6$Pt-10/Ph)**: A Schlenk flask was charged with **PtC$_6$Pt** (0.200 g, 0.099 mmol) and THF (40 mL). Solid Ph$_2$P(CH$_2$)$_{10}$PPh$_2$ (0.122 g, 0.238 mmol)[28] was added in one portion with stirring. After 12 h, the mixture was concentrated (to ≈15 mL) and ethanol (20 mL) was added. The solution was further concentrated (to ≈10 mL) and hexane (20 mL) was added. The precipitate was collected by filtration, washed with hexane (2×10 mL), and dried by oil pump vacuum to give **PtC$_6$Pt-10/Ph** as a light yellow solid (0.147 g, 0.081 mmol, 82%), decomp point 185°C (capillary, gradual darkening without melting). DSC: endotherm: $T_i = 201.0$, $T_e = 214.0$, $T_p = 232.5$, $T_c = 243.6$, $T_f = 249.2$°C; TGA (onset of mass loss): $T_i = 294.3$, $T_e = 301.1$, $T_f = 401.6$°C; ^1H NMR:[42] $\delta = 7.43$ (m, 16 H; o to P), 7.30 (m, 8 H; p to P), 7.23 (m, 16 H; m to P), 2.74 (m, 8 H; PCH_2), 2.09 (m, 8 H; PCH$_2$CH_2), 1.57 (m, 8 H; PCH$_2$CH$_2$CH_2), 1.39 ppm (m, 16 H; PCH$_2$CH$_2$CH$_2$CH_2CH_2); $^{13}C\{^1H\}$ NMR: $\delta = 147$ (br m, o to Pt), 137 (br m, m/p to Pt), 133.4 (virtual t, $^2J_{CP} = 5.6$ Hz, o to P), 132.5 (virtual t, $^1J_{CP} = 27.6$ Hz, i to P), 130.5 (s, p to P) 128.2 (virtual t, $^3J_{CP} = 4.9$ Hz, m to P), 95.7 (s, PtC≡C),[43] 95.2 (s, PtC≡C), 60.9 (s, PtC≡CC), 31.5 (virtual t, $^3J_{CP} = 7.5$ Hz, PCH$_2$CH$_2$), 29.9 (s, CH$_2$), 28.5 (virtual t, $^1J_{CP} = 18.4$ Hz, PCH_2), 28.3 (s, CH$_2$), 25.6 ppm (s, PCH$_2$CH$_2$); $^{31}P\{^1H\}$ NMR: $\delta = 14.5$ ppm (s, $^1J_{PPt} = 2594$ Hz);[41] IR (powder film): $\tilde{\nu} = 2104$ cm^{-1} (br w, C≡C); UV/Vis (CH$_2$Cl$_2$, 1.25×10^{-5} M): $\lambda(\varepsilon) = 313$ (51000), 343 (14000), 368 nm (8000 M^{-1} cm^{-1}); FAB-MS: m/z (%):[44] 1816 (100) [M−H]$^+$, 1649 (15) [M−C$_6$F$_5$]$^+$, 703 (20) [PtPPh$_2$(CH$_2$)$_{10}$PPh$_2$−2H]$^+$; elemental analysis calcd (%) for C$_{86}$H$_{80}$F$_{10}$P$_4$Pt$_2$: C 56.86 H 4.44; found: C 56.90, H 4.66.

***trans,trans*-[(C$_6$F$_5$){(Ph$_2$P(CH$_2$)$_{11}$PPh$_2$)}Pt(C≡C)$_3$Pt{(Ph$_2$P(CH$_2$)$_{11}$PPh$_2$)}(C$_6$F$_5$)] (PtC$_6$Pt-11/Ph)**: A Schlenk flask was charged with **PtC$_6$Pt** (0.019 g, 0.0094 mmol) and CH$_2$Cl$_2$ (94 mL). A solution of Ph$_2$P(CH$_2$)$_{11}$PPh$_2$ (0.012 g, 0.023 mmol)[28] in CH$_2$Cl$_2$ (110 mL) was passed through a silica gel pad (2 cm) directly into the Schlenk flask with stirring. After 16 h, the mixture was concentrated (to ≈100 mL) and ethanol (50 mL) was added. This step was repeated three times. The mixture was concentrated (to ≈5 mL). The precipitate was collected by filtration, washed with ethanol (3×3 mL), and dried by oil pump vacuum to give **PtC$_6$Pt-11/Ph** as a light yellow solid (0.012 g, 0.0065 mmol, 69%), decomp point 208°C (capillary, onset). ^1H NMR:[42] $\delta = 7.39$ (m, 16 H; o to P), 7.25 (m, 8 H; p to P), 7.17 (m, 16 H; m to P), 2.72 (m, 8 H; PCH_2), 2.07 (m, 8 H; PCH$_2$CH_2), 1.58–1.25 ppm (m, 28 H; remaining CH_2); $^{13}C\{^1H\}$ NMR: $\delta = 133.0$ (virtual t, $^2J_{CP} = 5.8$ Hz, o to P), 132.1 (virtual t, $^1J_{CP} = 27.5$ Hz, i to P), 130.0 (s, p to P), 127.8 (virtual t, $^3J_{CP} = 5.1$ Hz, m to P), 94.6 (s, PtC≡C),[43,45] 60.3 (s, PtC≡CC), 30.5 (virtual t, $^3J_{CP} = 7.7$ Hz, PCH$_2$CH$_2$), 28.6 (virtual t, $^1J_{CP} = 18.3$ Hz, PCH_2), 28.2 (s, CH$_2$), 28.1 (s, CH$_2$), 27.6 (s, CH$_2$), 26.1 ppm (s, PCH$_2$CH_2); $^{31}P\{^1H\}$ NMR: $\delta = 15.3$ ppm (s, $^1J_{PPt} = 2606$ Hz).[41] IR (powder film): $\tilde{\nu} = 2108$ cm^{-1} (w, C≡C); FAB-MS: m/z (%):[44] 1845 (100) [M]$^+$, 1678 (12) [M−C$_6$F$_5$]$^+$.

***trans,trans*-[(C$_6$F$_5$){(Ph$_2$P(CH$_2$)$_{12}$PPh$_2$)}Pt(C≡C)$_3$Pt{(Ph$_2$P(CH$_2$)$_{12}$PPh$_2$)}(C$_6$F$_5$)] (PtC$_6$Pt-12/Ph)**: A Schlenk flask was charged with **PtC$_6$Pt** (0.114 g, 0.056 mmol) and THF (30 mL). Solid Ph$_2$P(CH$_2$)$_{12}$PPh$_2$ (0.073 g, 0.14 mmol)[28] was added in one portion with stirring. After 16 h, the mixture was concentrated (to ≈10 mL) and ethanol (20 mL) was added. The mixture was further concentrated (to ≈15 mL) and hexane (15 mL) was added. The precipitate was collected by filtration, washed with hexane (2×10 mL), and dried by oil pump vacuum to give **PtC$_6$Pt-12/Ph** as a yellow solid (0.063 g, 0.032 mmol, 57%), decomp point 171°C (capillary, gradual darkening without melting). DSC: endotherm: $T_i = 205.3$, $T_e = 225.4$, $T_c = 244.5$, $T_f = 247.6$°C; TGA (onset of mass loss): $T_i = 271.1$, $T_e = 283.0$, $T_f = 401.8$°C; ^1H NMR:[42a,46] $\delta = 7.40$ (m, 16 H; o to P), 7.19 (m, 24 H; m/p to P), 2.65 (m, 8 H; PCH_2), 2.35 (s, 8 H; PCH$_2$CH_2), 1.41 (m, 16 H; PCH$_2$CH$_2$CH_2), 1.23 ppm (m, 16 H; PCH$_2$CH$_2$CH$_2$CH$_2$CH_2); $^{31}P\{^1H\}$ NMR: $\delta = 16.3$ ppm (s, $^1J_{PPt} = 2609$ Hz).[41] IR (powder film): $\tilde{\nu} = 2123$ cm^{-1} (br w, C≡C); FAB-MS: m/z (%):[44] 1873 (100) [M]$^+$, 1705 (5) [M−C$_6$F$_5$]$^+$; elemental analysis calcd (%) for C$_{90}$H$_{88}$F$_{10}$P$_4$Pt$_2$: C 57.69, H 4.73; found: C 57.79, H 4.86.

***trans,trans*-[(C$_6$F$_5$){(*p*-tol$_2$P(CH$_2$)$_{14}$P*p*-tol$_2$)}Pt(C≡C)$_3$Pt{(*p*-tol$_2$P-(CH$_2$)$_{14}$P*p*-tol$_2$)}(C$_6$F$_5$)] (PtC$_6$Pt-14/*p*-tol)**: A Schlenk flask was charged with **PtC$_6$Pt** (0.090 g, 0.045 mmol) and THF (25 mL). Solid *p*-tol$_2$P-(CH$_2$)$_{14}$P*p*-tol$_2$ (0.066 g, 0.11 mmol)[29] was added in one portion with stirring. After 6 h, the mixture was concentrated under vacuum and ethanol

(30 mL) was added. The mixture was further concentrated (to ≈15 mL). The precipitate was collected by filtration, washed with ethanol (2× 5 mL), and dried by oil pump vacuum to give **PtC₆Pt-14/p-tol** as a yellow solid (0.052 g, 0.025 mmol, 57%), decomp point 183°C (capillary, gradual darkening without melting). DSC: endotherm: $T_i = 154.0$, $T_e = 165.1$, $T_p = 181.5$, $T_c = 209.3$, $T_f = 209.3°C$; TGA (onset of mass loss): $T_i = 285.5$, $T_e = 294.0$, $T_f = 401.4°C$; ¹H NMR:[42] $\delta = 7.26$ (m, 16H; o to P), 6.97 (br d, $^3J_{HH} = 7.8$ Hz, 16H; m to P), 2.63 (m, 8H; PCH_2), 2.27 (s, 24H; CH_3), 1.98 (m, 8H; PCH₂CH_2), 1.50 (m, 8H; PCH₂CH₂CH_2), 1.33 (m, 16H; PCH₂CH₂CH₂CH_2CH_2), 1.24 ppm (m, 16H; PCH₂CH₂CH₂CH₂CH₂CH_2CH_2); ¹³C{¹H} NMR: $\delta = 140.5$ (s, p to P), 133.3 (virtual t, $^2J_{CP} = 5.9$ Hz, o to P), 129.0 (virtual t, $^1J_{CP} = 28.5$ Hz, i to P), 128.8 (virtual t, $^3J_{CP} = 5.2$ Hz, m to P), 95.3 (s, PtC≡C),[43,45] 60.8 (s, PtC≡CC), 30.7 (virtual t, $^3J_{CP} = 7.7$ Hz, PCH₂CH₂CH_2), 29.2 (CH_2), 28.7 (CH_2), 28.6 (CH_2), 28.5 (overlapping virtual t, PCH_2), 28.3 (s, CH_2), 26.1 (s, PCH₂CH_2), 21.6 ppm (s, CH_3); ³¹P{¹H} NMR: $\delta = 14.2$ ppm (s, $^1J_{PPt} = 2578$ Hz);[41] ¹⁹F{¹H} NMR: $\delta = -117.8$ (m, 4F, $^3J_{FPt} = 282$ Hz,[41] o to Pt), −166.0 (m, 4F, m to Pt), −166.5 ppm (t, 2F, $^3J_{FF} = 17$ Hz, p to Pt); IR (powder film): $\tilde{v} = 2104$ cm⁻¹ (br w, C≡C); UV/Vis (CH₂Cl₂, 1.25 × 10⁻⁵ M): $\lambda(\varepsilon) = 323$ (30000), 343 (13000), 367 nm (8000 M⁻¹ cm⁻¹); FAB-MS: m/z (%):[44] 2041 (100) $[M]^+$, 1874 (<1) $[M-C_6F_5]^+$, 817 (15) $[PtPtol_2(CH_2)_{14}Ptol_2]^+$; elemental analysis calcd (%) for C₁₀₂H₁₁₂F₁₀P₄Pt₂: C 59.99, H 5.53; found: C 60.39, H 5.61.

***trans,trans*-[(C₆F₅){(p-tBuC₆H₄)₂P(CH₂)₁₄P(p-C₆H₄-tBu)₂}Pt(C≡C)₃Pt{(p-tBuC₆H₄)₂P(CH₂)₁₄P(p-C₆H₄-tBu)₂}(C₆F₅)] (PtC₆Pt-14/p-C₆H₄-tBu)**: A Schlenk flask was charged with **PtC₆Pt** (0.200 g, 0.099 mmol) and THF (40 mL). Solid (p-tBuC₆H₄)₂P(CH₂)₁₄P(p-C₆H₄-tBu)₂ (0.200 g, 2.48 mmol)[29] was added in one portion with stirring. After 12 h, the mixture was concentrated under vacuum and ethanol (30 mL) was added. The mixture was further concentrated (to ≈15 mL). The precipitate was collected by filtration, washed with ethanol (2×15 mL), and dried by oil pump vacuum to give **PtC₆Pt-14/p-C₆H₄-tBu** as a yellow solid (0.169 g, 0.071 mmol, 71%), decomp point 234°C (capillary, some softening and then gradual darkening). TGA (onset of mass loss): $T_i = 278.7$, $T_f = 401.3°C$; ¹H NMR:[42a] $\delta = 7.35$ (m, 16H; o to P), 7.20 (br d, $^3J_{HH} = 7.9$ Hz, 16H; m to P), 2.73 (m, 8H; PCH_2), 2.00 (m, 8H; PCH₂CH_2), 1.53 (m, 8H; PCH₂CH₂CH_2), 1.36 (m, 16H; PCH₂CH₂CH₂CH_2CH_2), 1.33 (m, 16H; PCH₂CH₂CH₂CH₂CH₂CH_2CH_2), 1.26 ppm (s, 72H; tBu); ³¹P{¹H} NMR: $\delta = 13.9$ ppm (s, $^1J_{PPt} = 2566$ Hz);[41] IR (powder film): $\tilde{v} = 2100$ cm⁻¹ (br w, C≡C); FAB-MS: m/z (%):[44] 2377 (90) $[M]^+$, 2210 (<1) $[M-C_6F_5]^+$, 984 (100) $[(BuC_6H_4)_2P(CH_2)_{14}P(C_6H_4Bu)_2]^+$; elemental analysis calcd (%) for C₁₂₆H₁₆₀F₁₀P₄Pt₂: C 63.62, H 6.78; found: C 62.83, H 6.79.

***trans,trans*-[(C₆F₅){(Ph₂P(CH₂)₁₆PPh₂)}Pt(C≡C)₃Pt{(Ph₂P(CH₂)₁₆PPh₂)}-(C₆F₅)] (PtC₆Pt-16/Ph)**: A Schlenk flask was charged with **PtC₆Pt** (0.143 g, 0.071 mmol) and THF (30 mL). Solid Ph₂P(CH₂)₁₆PPh₂ (0.101 g, 0.169 mmol)[28] was added in one portion with stirring. After 6 h, a ³¹P NMR spectrum was recorded ($\delta = 14.5$, s).[47] The mixture was concentrated (to ≈10 mL) and ethanol (20 mL) was added. The mixture was further concentrated (to ≈15 mL). The precipitate was collected by filtration, washed with hexane (2×10 mL) and dried by oil pump vacuum to give oligomerized **PtC₆Pt-16/Ph** as a light yellow insoluble solid (0.089 g, 0.045 mmol, 64%); IR (powder film): $\tilde{v} = 2108$ cm⁻¹ (br w, C≡C); FAB-MS: m/z (%):[44] 1986 (100) $[M-H]^+$; elemental analysis calcd (%) for C₉₈H₁₀₄F₁₀P₄Pt₂: C 59.27, H 5.27; found: C 59.30, H 5.36.

***trans,trans*-[(C₆F₅){(Ph₂P(CH₂)₈PPh₂)}Pt(C≡C)₂Pt{(Ph₂P(CH₂)₈PPh₂)}-(C₆F₅)] (PtC₄Pt-8/Ph)**: A Schlenk flask was charged with **PtC₄Pt** (0.052 g, 0.026 mmol) and CH₂Cl₂ (52 mL). A solution of Ph₂P(CH₂)₈PPh₂ (0.031 g, 0.064 mmol)[28] in CH₂Cl₂ (32 mL) was passed through a silica gel pad (2 cm) directly into the Schlenk flask with stirring. After 16 h, the solvent was removed by oil pump vacuum. The residue was chromatographed (25 cm silica gel column, 20:80 v/v CH₂Cl₂/hexanes). The solvent was removed from the product-containing fractions by rotary evaporation. The residue was recrystallized from hexanes and dried by oil pump vacuum to give **PtC₄Pt-8/Ph** as a light yellow solid (0.024 g, 0.014 mmol, 53%), decomp point 160°C (capillary, onset). ¹H NMR:[42] $\delta = 7.40$ (m, 16H; o to P), 7.22 (m, 8H; p to P), 7.11 (m, 16H; m to P), 2.64 (m, 8H; PCH_2), 1.99 (m, 8H; PCH₂CH_2), 1.55 (m, 8H; PCH₂CH₂CH_2), 1.42 ppm

(m, 8H; remaining CH_2); ¹³C{¹H} NMR: $\delta = 145.8$ (dd, $^1J_{CF} = 222$ Hz, $^2J_{CF} = 22$ Hz, o to Pt), 136.1 (dm, $^1J_{CF} = 240$ Hz, m/p to Pt), 133.0 (virtual t, $^2J_{CP} = 5.5$ Hz, o to P), 132.2 (virtual t, $^1J_{CP} = 27.0$ Hz, i to P), 129.7 (s, p to P), 127.5 (virtual t, $^3J_{CP} = 4.9$ Hz, m to P), 99.9 (s, PtC≡C),[43] 87.0 (s, PtC≡C),[43] 30.6 (virtual t, $^3J_{CP} = 7.1$ Hz, PCH₂CH₂CH_2), 27.6 (virtual t, $^1J_{CP} = 18.1$ Hz, PCH_2), 27.1 (s, PCH₂CH₂CH_2), 24.3 ppm (s, PCH₂CH_2); ¹⁹F{¹H} NMR: $\delta = -117.11$ (m, $^3J_{FPt} = 286$ Hz, 4F, o to Pt), −164.5 to −165.1 ppm (m, 6F, m/p to Pt); ³¹P{¹H} NMR: $\delta = 13.7$ ppm (s, $^1J_{PPt} = 2621$ Hz).[41] IR (powder film): $\tilde{v} = 3057$ (w), 2930 (m), 2856 (w), 1498 (s), 1455 (s), 1436 (m), 1355 (w), 1262 (m), 1104 (m), 1054 (s), 1027 (m), 950 (vs), 787 (s), 737 (s), 687 (vs); UV/Vis (CH₂Cl₂, 1.25 × 10⁻⁵ M): $\lambda(\varepsilon) = 317$ nm (20600 M⁻¹ cm⁻¹); FAB-MS: m/z (%):[44] 1736 (63) $[M]^+$, 1570 (8) $[M-C_6F_5+H]^+$, 675 (100) $[Pt(Ph_2P(CH_2)_8PPh_2-2H]^+$, 379 (41) $[Pt(Ph_2P)-H]^+$, 302 (82) $[Pt(PhP)-H]^+$.

***trans,trans*-[(C₆F₅){(p-tol₂P(CH₂)₈P p-tol₂)}Pt(C≡C)₂Pt{(p-tol₂P(CH₂)₈P p-tol₂)}(C₆F₅)] (PtC₄Pt-8/p-tol)**: A Schlenk flask was charged with **PtC₄Pt** (0.095 g, 0.050 mmol) and CH₂Cl₂ (100 mL). A solution of p-tol₂P-(CH₂)₈P p-tol₂ (0.067 g, 0.13 mmol)[29] in CH₂Cl₂ (65 mL) was passed through a silica gel pad (2 cm) directly into the Schlenk flask with stirring. After 12 h, the mixture was concentrated (to ≈80 mL), and ethanol (50 mL) was added. This step was repeated three times. The solvent was removed by oil pump vacuum. The residue was extracted with hexanes. The extract was filtered through a silica gel pad (2 cm; hexanes, then CH₂Cl₂). The solvent was removed by oil pump vacuum. The extraction, filtration, and solvent removal steps were repeated twice to give **PtC₄Pt-8/p-tol** as a light yellow solid (0.080 g, 0.043 mmol, 87%; purity see text). ¹H NMR:[42] $\delta = 7.29$ (m, 16H; o to P), 6.92 (br d, $^3J_{HH} = 7.8$ Hz, 16H; m to P), 2.60 (m, 8H; PCH_2), 2.26 (s, 24H; CH_3), 1.94 (m, 8H; PCH₂CH_2), 1.53 (m, 8H; PCH₂CH₂CH_2), 1.40 (br m, 8H; remaining CH_2); ¹³C{¹H} NMR: $\delta = 145.9$ (dd, $^1J_{CF} = 225$ Hz, $^2J_{CF} = 22$ Hz, o to Pt), 139.8 (s, p to P), 136.3 (dm, $^1J_{CF} = 247$ Hz, m/p to Pt), 133.0 (virtual t, $^2J_{CP} = 5.9$ Hz, o to P), 128.9 (virtual t, $^1J_{CP} = 27.8$ Hz, i to P), 128.2 (virtual t, $^3J_{CP} = 5.1$ Hz, m to P), 99.8 (s, $^2J_{CPt} = 265$ Hz,[41] PtC≡C), 87.2 (s, $^1J_{CPt} = 970$ Hz,[41] PtC≡C), 30.7 (virtual t, $^3J_{CP} = 7.3$ Hz, PCH₂CH₂CH_2), 27.8 (virtual t, $^1J_{CP} = 18.3$ Hz, PCH_2), 27.2 (s, PCH₂CH₂CH_2), 24.2 ppm (s, PCH₂CH_2); ³¹P{¹H} NMR: $\delta = 12.2$ ppm (s, $^1J_{PPt} = 2604$ Hz);[41] IR (powder film): $\tilde{v} = 2926$ (m), 2856 (w), 1602 (w), 1498 (m), 1451 (m), 1100 (s), 1054 (s), 953 (s), 802 (vs), 710 cm⁻¹ (m).

Crystallography:[48] A) A solution of **PtC₆Pt** in THF was layered with methanol and stored at room temperature. After three days, the resulting yellow blocks that were produced were used for data collection as outlined in Table 1. Cell parameters were obtained from 10 frames using a 10° scan and refined with 10822 reflections. Lorentz, polarization, and absorption corrections[49] were applied. The space group was determined from systematic absences and subsequent least-squares refinement. The structure was solved by direct methods. The parameters were refined with all data by full-matrix-least-squares on F^2 using SHELXL-97.[50] Non-hydrogen atoms were refined with anisotropic thermal parameters. The hydrogen atoms were fixed in idealized positions by means of a riding model. Scattering factors were taken from the literature.[51] The crystal contained four molecules of THF per molecule of **PtC₆Pt**. The structure exhibited an inversion center at the midpoint of the C₆ chain. B) A solution of **Pt′C₆Pt′** in CH₂Cl₂ was layered with hexane and stored at room temperature. After two days, the yellow prisms were analyzed as described for **PtC₆Pt** (refined with 5841 reflections). The structure was solved and refined in an identical manner, and exhibited an inversion center at the midpoint of the C₆ chain. C) A solution of **PtC₆Pt-10/Ph** in CH₂Cl₂ was layered with methanol and stored at room temperature. After three days, the yellow blocks were analyzed as described for **PtC₆Pt** (refined with 8703 reflections). The structure was solved and refined in an identical manner, and exhibited an inversion center at the midpoint of the C₆ chain. D) A solution of **PtC₆Pt-11/Ph** in CH₂Cl₂ was layered with methanol and stored at room temperature. After four days, the yellow crystals were analyzed as described for **PtC₆Pt** (refined with 9539 reflections). The structure was solved and refined in an identical manner. The crystal contained two molecules of CH₂Cl₂ per molecule of **PtC₆Pt-11/Ph**. The structure exhibited an inversion center at the midpoint of the C₆ chain. E) A solution of **PtC₆Pt-14/p-tol** in CH₂Cl₂ was layered with methanol and stored at room temperature. After three days,

the yellow prisms were analyzed as described for **PtC₆Pt** (refined with 21 967 reflections). The structure was solved and refined in an identical manner. The crystal contained two molecules of CH_2Cl_2 per molecule of **PtC₆Pt-14/*p*-tol**. The methylene groups C3a/C3a′ and C8a/C8a′ were disordered and refined to 79:21 and 46:54 occupancy ratios, respectively. F) Ethanol vapor was allowed to diffuse into a solution of **PtC₄Pt** in toluene at room temperature. After five days, the yellow prisms were analyzed as described for **PtC₆Pt** (refined with 19 142 reflections). The structure was solved and refined in an identical manner. A strong residual electron density close to Pt2/C4 was considered to be an artifact of the crystal quality, and affected the parameters for C4.

Acknowledgements

[1] M. I. Bruce, P. J. Low, *Adv. Organomet. Chem.* **2004**, *50*, 179.

[2] F. Paul, C. Lapinte in *Unusual Structures and Physical Properties in Organometallic Chemistry* (Eds.: M. Gielen, R. Willem, B. Wrackmeyer), Wiley, New York, **2002**, pp. 220–291.

[3] a) S. Szafert, J. A. Gladysz, *Chem. Rev.* **2003**, *103*, 4175; b) S. Szafert, J. A. Gladysz, *Chem. Rev.* **2006**, *106*, PR1.

[4] R. Dembinski, T. Bartik, B. Bartik, M. Jaeger, J. A. Gladysz, *J. Am. Chem. Soc.* **2000**, *122*, 810.

[5] W. Mohr, J. Stahl, F. Hampel, J. A. Gladysz, *Chem. Eur. J.* **2003**, *9*, 3324.

[6] Q. Zheng, J. C. Bohling, T. B. Peters, A. C. Frisch, F. Hampel, J. A. Gladysz, *Chem. Eur. J.* **2006**, *12*, 6486.

[7] a) G. Schermann, T. Grösser, F. Hampel, A. Hirsch, *Chem. Eur. J.* **1997**, *3*, 1105; b) T. Gibtner, F. Hampel, J.-P. Gisselbrecht, A. Hirsch, *Chem. Eur. J.* **2002**, *8*, 408; c) T. Luu, E. Elliot, A. D. Slepkov, S. Eisler, R. McDonald, F. A. Hegmann, R. R. Tykwinski, *Org. Lett.* **2005**, *7*, 51; d) S. Eisler, A. D. Slepkov, E. Elliot, T. Luu, R. McDonald, F. A. Hegmann, R. R. Tykwinski, *J. Am. Chem. Soc.* **2005**, *127*, 2666; e) C. Klinger, O. Vostrowsky, A. Hirsch, *Eur. J. Org. Chem.* **2006**, 1508.

[8] a) S. M. ALQaisi, K. J. Galat, M. Chai, D. G. Ray, III, P. L. Rinaldi, C. A. Tessier, W. J. Youngs, *J. Am. Chem. Soc.* **1998**, *120*, 12149 b) M. I. Bruce, K. Costuas, J.-F. Halet, B. C. Hall, P. J. Low, B. K. Nicholson, B. W. Skelton, A. H. White, *J. Chem. Soc. Dalton Trans.* **2002**, 383 c) M. Janka, G. K. Anderson, N. P. Rath, *Organometallics* **2004**, *23*, 4382.

[9] Computational study: F. Zhuravlev, J. A. Gladysz, *Chem. Eur. J.* **2004**, *10*, 6510.

[10] For other Pt(C≡C)ₙPt complexes (*n*=2–4), see a) A. Klein, K.-W. Klinkhammer, T. Scheiring, *J. Organomet. Chem.* **1999**, *592*, 128; b) C. Müller, R. J. Lachicotte, W. D. Jones, *Organometallics* **2002**, *21*, 1190; c) W.-Y. Wong, C.-K. Wong, G.-L. Lu, K.-W. Cheah, J.-X. Shi, Z. Lin, *J. Chem. Soc. Dalton Trans.* **2002**, 4587 d) V. W.-W. Yam, K. M.-C. Wong, N. Zhu, *Angew. Chem.* **2003**, *115*, 1438; *Angew. Chem. Int. Ed.* **2003**, *42*, 1400.

[11] G. R. Owen, F. Hampel, J. A. Gladysz, *Organometallics* **2004**, *23*, 5893.

[12] Q. Zheng, F. Hampel, J. A. Gladysz, *Organometallics* **2004**, *23*, 5896.

[13] J. Stahl, W. Mohr, L. de Quadras, T. B. Peters, J. C. Bohling, J. M. Martín-Alvarez, G. R. Owen, F. Hampel, J. A. Gladysz, *J. Am. Chem. Soc.* **2007**, *129*, 8282.

[14] L. de Quadras, E. B. Bauer, W. Mohr, J. C. Bohling, T. B. Peters, J. Martín-Alvarez, F. Hampel, J. A. Gladysz, *J. Am. Chem. Soc.* **2007**, *129*, 8296.

[15] L. de Quadras, E. B. Bauer, J. Stahl, F. Zhuravlev, F. Hampel, J. A. Gladysz, *New J. Chem.* **2007**, *31*, 1537.

[16] Review: M. J. Frampton, H. L. Anderson, *Angew. Chem.* **2007**, *119*, 1046; *Angew. Chem. Int. Ed.* **2007**, *46*, 1028; .

[17] a) M. Ohkita, J.-M. Lehn, G. Baum, D. Fenske, *Chem. Eur. J.* **1999**, *5*, 3471; b) D. M. Bassani, J.-M. Lehn, *Bull. Soc. Chim. Fr.* **1997**, *134*, 897.

[18] More exactly, a diastereotopic group in one enantiomer exchanges with the other in the opposite enantiomer.

[19] E. L. Eliel, S. H. Wilen, *Stereochemistry of Organic Compounds*, Wiley-Interscience, New York, **1994**, pp. 1142–1155.

[20] a) S. Arulmozhiraja, T. Fujii, *J. Chem. Phys.* **2001**, *115*, 10589, and references therein. b) K. Müllen, W. Heinz, F.-G. Klärner, W. R. Roth, I. Kindermann, O. Adamczak, M. Wette, J. Lex, *Chem. Ber.* **1990**, *123*, 2349.

[21] a) G. Brizius, K. Billingsley, M. D. Smith, U. H. F. Bunz, *Org. Lett.* **2003**, *5*, 3951; b) S. Toyota, T. Iida, C. Kunizane, N. Tanifuji, Y. Yoshida, *Org. Biomol. Chem.* **2003**, *1*, 2298; c) T. Makino, S. Toyota, *Bull. Chem. Soc. Jpn.* **2005**, *78*, 917; d) S. Toyota, T. Yanagihara, Y. Yoshida, M. Goichi, *Bull. Chem. Soc. Jpn.* **2005**, *78*, 1351; e) O. S. Miljanić, S. Han, D. Holmes, G. R. Schaller, K. P. C. Vollhardt, *Chem. Commun.* **2005**, 2606; f) R. Nandy, M. Subramoni, B. Varghese, S. Sankararaman, *J. Org. Chem.* **2007**, *72*, 938.

[22] Endgroup–endgroup interactions lead to rotational barriers of 11–12 kcal mol⁻¹ in octahedral/square planar ReC≡CPd and ReC≡CRh systems: W. Weng, T. Bartik, M. Brady, B. Bartik, J. A. Ramsden, A. M. Arif, J. A. Gladysz, *J. Am. Chem. Soc.* **1995**, *117*, 11922.

[23] G. R. Owen, J. Stahl, F. Hampel, J. A. Gladysz, *Organometallics* **2004**, *23*, 5889.

[24] J. Stahl, Doctoral Thesis, Universität Erlangen-Nürnberg, **2003**.

[25] Many Fe(C≡C)ₙH and FeCl complexes undergo efficient cross-coupling when treated with KPF₆/*t*BuOK: F. Coat, M. Guillemot, F. Paul, C. Lapinte, *J. Organomet. Chem.* **1999**, *578*, 76, and references therein.

[26] a) E. B. Bauer, F. Hampel, J. A. Gladysz, *Organometallics* **2003**, *22*, 5567; b) T. Shima, E. B. Bauer, F. Hampel, J. A. Gladysz, *Dalton Trans.* **2004**, 1012.

[27] The crystal structure of the analog of **Pt′C₆Pt′** in which the pentafluorophenyl ligands are replaced by phenyl ligands has also been reported in ref. [10c].

[28] W. Mohr, C. R. Horn, J. Stahl, J. A. Gladysz, *Synthesis* **2003**, 1279.

[29] L. de Quadras, J. Stahl, F. Zhuravlev, J. A. Gladysz, *J. Organomet. Chem.* **2007**, *692*, 1859.

[30] The gross structures of these oligomers can be proved by adding an excess of PEt₃, which gives the independently synthesized complexes *trans,trans*-[(C₆F₅){(Et₃P)₂}Pt(C≡C)ₙPt{(PEt₃)₂}(C₆F₅)] (**Pt′CₓPt′**)- (ref. [13]).

[31] J. S. Siegel, F. A. L. Anet, *J. Org. Chem.* **1988**, *53*, 2629.

[32] A. Bondi, *J. Phys. Chem.* **1964**, *68*, 441.

[33] H. Friebolin, *Basic One- and Two-Dimensional NMR Spectroscopy*, 4th Ed., Wiley-VCH, Weinheim, Germany, **2005**, Chapter 11.2.

[34] H. K. Cammenga, M. Epple, *Angew. Chem.* **1995**, *107*, 1284; *Angew. Chem. Int. Ed. Engl.* **1995**, *34*, 1171. The T_e values best represent the temperature of the endotherm or exotherm.

[35] a) A. Klein, W. Kaim, *Organometallics* **1995**, *14*, 1176; b) A. Klein, S. Hasenzahl, W. Kaim, J. Fiedler, *Organometallics* **1998**, *17*, 3532.

[36] a) S. Leininger, B. Olenyuk, P. J. Stang, *Chem. Rev.* **2000**, *100*, 853; b) M. Fujita, M. Tominaga, A. Hori, B. Therrien, *Acc. Chem. Res.* **2005**, *38*, 369.

[37] In the complex designated as **PtC₈Pt-16/Ph** in Table 6, two of the four PtPAr₂CH₂CH₂ segments are gauche. There is one such segment in one solvate of **PtC₈Pt-10/Ph**, (ref. [13]) and none in any other complexes of the type **PtCₓPt-*m*/Ar** (*x*=6, 8, 12).

[38] R. W. Hoffmann, *Angew. Chem.* **2000**, *112*, 2134; *Angew. Chem. Int. Ed.* **2000**, *39*, 2054.

[39] Although this study has been concluded, we continue to speculate whether a shorter sp³ chain, such as in **PtC₄Pt-6/Ph**, might have afforded a D_2 helical ground state.

[40] H. Kuhn, N. Weisbach, unpublished results, Universität Erlangen-Nürnberg.

FULL PAPER

[41] This coupling represents a satellite (d, $^{195}Pt = 33.8\%$), and is not reflected in the peak multiplicity given.

[42] a) All complexes exhibit characteristic patterns of aryl ^1H and ^{13}C NMR signals. Assignments were made by analogy to related compounds described earlier in references [5,13,14]. b) Complexes with PtPAr$_2$CH$_2$CH$_2$CH$_2$ linkages exhibit characteristic ^{13}C NMR chemical shift and coupling constant patterns. In earlier studies in references [13,15], assignments were confirmed by ^1H,^{13}C and ^1H,^1H COSY spectra. Those in this paper have been made by analogy. See also footnote 42 in reference [26a]; c) For virtual triplets (W. H. Hersh, *J. Chem. Educ.* **1997**, *74*, 1485), the *J* values represent the *apparent* couplings between adjacent peaks. d) Except for **Pt′C₆Pt′**, the *ipso* and/or other C$_6$F$_5$ ^{13}C NMR signals were not observed.

[43] Platinum coupling would be expected based upon spectra of related compounds; however, the signal/noise ratio was not sufficient.

[44] Values correspond to the most intense peaks of the isotope envelope. In some cases, background peaks from the NBA matrix were more intense than the molecular ion.

[45] The PtC≡C ^{13}C NMR signals of **PtC₆Pt** have similar chemical shifts[5] and were not always resolved in **PtC₆Pt-*m*/Ar**.

[46] This complex was too insoluble for a ^{13}C NMR spectrum.

[47] An analogous experiment with Ph$_2$P(CH$_2$)$_{18}$PPh$_2$ (ref. [28]) gave a reaction mixture with a single signal at $\delta = 14.5$ ppm (s).

[48] CCDC 258714 (**PtC₆Pt·4THF**), 649045 (**Pt′C₆Pt′**), 258717 (**PtC₆Pt-10/Ph**), 258715 (**PtC₆Pt-11/Ph·2CH₂Cl₂**), 258716 (**PtC₆Pt-14/*p*-tol·2CH₂Cl₂**), and 649046(**PtC₄Pt**) contain the supplementary crystallographic data for this paper. These data can be obtained free of charge from The Cambridge Crystallographic Data Centre via www.ccdc.cam.ac.uk/data_request/cif.

[49] a) "Collect" data collection software, B. V. Nonius, **1998**; b) "Scalepack" data processing software: Z. Otwinowski, W. Minor, *Methods Enzymol.* **1997**, *276*, 307.

[50] G. M. Sheldrick, SHELX-97, Program for refinement of crystal structures, University of Göttingen, **1997**.

[51] D. T. Cromer, J. T. Waber in *International Tables for X-ray Crystallography*, (Eds.: J. A. Ibers, W. C. Hamilton), Kynoch, Birmingham, England, **1974**.